TRACK FOLLOWING CONTROL OF HDD DUAL-STAGE ACTUATOR USING QUANTITATIVE FEEDBACK THEORY

TAWEESAK ARYURAWATTANA

A THESIS SUBMITTED IN PARTIAL FULFILLMENT

OF THE REQUIREMENT FOR THE DEGREE OF

MASTER OF ENGINEERING IN DATA STORAGE TECHNOLOGY AND INNOVATIONS (INTERNATIONAL PROGRAM)

INTERNATIONAL COLLEGE

KING MONGKUT'S INSTITUTE OF TECHNOLOGY LADKRABANG

2013

KMITL-2013-IC-M-005-002

Thesis title:	Track Following Control Of HDD Dual-Stage Actuator Using Quantitative Feedback Theory
Student:	Mr. Taweesak Aryurawattana
Student ID:	52600619
Degree:	Master degree of engineering
Program:	Data storage technology and applications
Year:	2013
Thesis advisor:	Assoc. Prof. Dr. Unnat Pinsopon
Co,Thesis advisor:	Assoc. Prof. Dr. Withit Chatlatanagulchai (KU)

ABSTRACT

The trend of head disk drive (HDD) requires the increasing of areal density, resulting in smaller bit size and smaller media track pitch. The controller design of the read/write head servo- mechanism has to achieve both track-seeking and track-following. This paper deals only with track-following control of the read/write head in order that the head stays in the middle of the track. Data must be able read or written within the boundary of ±10% of the track width in the presence of external disturbance. The control design for track following must have an ability to reject disturbance, which in turn, could increase the hard disk drive capacity. In this thesis study, quantitative feedback theory is proposed as the track following control scheme. The plant identification of the dual-stage actuator and the controller design were done on frequency domain. All the works were completed using Matlab tools for design and simulation. The proposed control technique is able to reduce 50% of settling time and is thirty times more capable in attenuating repeatable runout disturbance compared with the conventional PID control technique.

ACKNOWLEDGEMENTS

Many thanks to my advisor at College of Data Storage Technology and Application, King Mongkut's Institute of Technology Ladkrabang: Asst. Prof. Dr. Unnat Pinsopon (KMITL) for offering valuable advice, support and guidance throughout my Masters study, Assoc. Prof. Dr. Withit Chatlatanagulchai (KU) for offering valuable advice, about Quantitative Feedback Theory, Craig Borghesani and Terasoft, Inc for their evaluation copy of the QFT Matlab toolbox.

Many thanks to my colleagues at Western Digital (Thailand) on the valuable comments help and support during my Masters study. Appreciation also goes to my supervisor in the Servo Engineering organization for supporting my Masters study. Special appreciation goes to Tawan and the Senior Management team at Western Digital (Thailand) for granting this scholarship and opportunity, without which I would not have completed my Masters study.

I would also like to thank my parents and family for the support all these years.

Taweesak Aryurawattana

CONTENTS

LIST OF FIGURES

LIST OF FIGURES (CONT.)

LIST OF TABLES

CHAPTER 1

Introduction

1.1 Background and Problems

The Hard Disk Drive (HDD) is a data storage which uses magnetic field component to store digital information. The HDD industry is challenged to keep developing new technology for catching up the market demand of higher areal density HDD. Advance magnetic fields, material science, electronics, motor technology, servo mechanism, tribology, signal processing and robust process control in manufacturing are all important factors for HDD industry to achieve the demand goal. In order to increase the HDD capacity without increasing the hardware size, the HDD read/write head servo-mechanism is one of the areas to be addressed. The HDD head controller could be developed to utilize the HDD media more efficiently, hence increasing the HDD capacity.

In most commercial HDD, rotation disks of recoding magnetic media are written with data that are arranged in concentric circles or data track. The datum are read or written to magnetic media by read/write heads. In order to accomplish the positioning of the read/write head positioning, there are two parts to be considered: the mechanical part and the servo controller part.

For the mechanical part, an actuator concentrically moves the read/write head from the current the track to the target track. The actuator conventionally used in HDD is the voice coil motor (VCM). The VCM itself has a low bandwidth frequency. With the application of the closed loop control technique, its bandwidth could be extended. This characteristic would affect the positioning accuracy at high areal density. In order to develop a high bandwidth actuator, a dual-stage has been proposed [4]. In the dual-stage actuator, a micro actuator is mounted on a larger conventional VCM actuator. More detail will be explained in chapter 3.

The servo controller used in conventional HDD is the PID controllers which achieve the head positioning accuracy at the present demand. However with the trend that HDD must increase the areal density by the rate of 100% per year, the PID controller might be the bottom neck of the drive for its high overshoot and poor disturbance rejection at small track pitch. Instead, other competent techniques would be challenging tools to achieve the goal.

The quantitative feedback theory (QFT) is one of the potential solutions to achieve the servo control at small track pitch. Based on literature reviews, the QFT gave better performance on overshoots and disturbance rejection, to be explained in more detail chapter 2.

1.2 Problem Statement

Figure 1.1 shows the growing trend of hard disk drive areal density [24]. According to the trend, the HDD areal density at the present time is increasing at a rate of 100% per year [24].

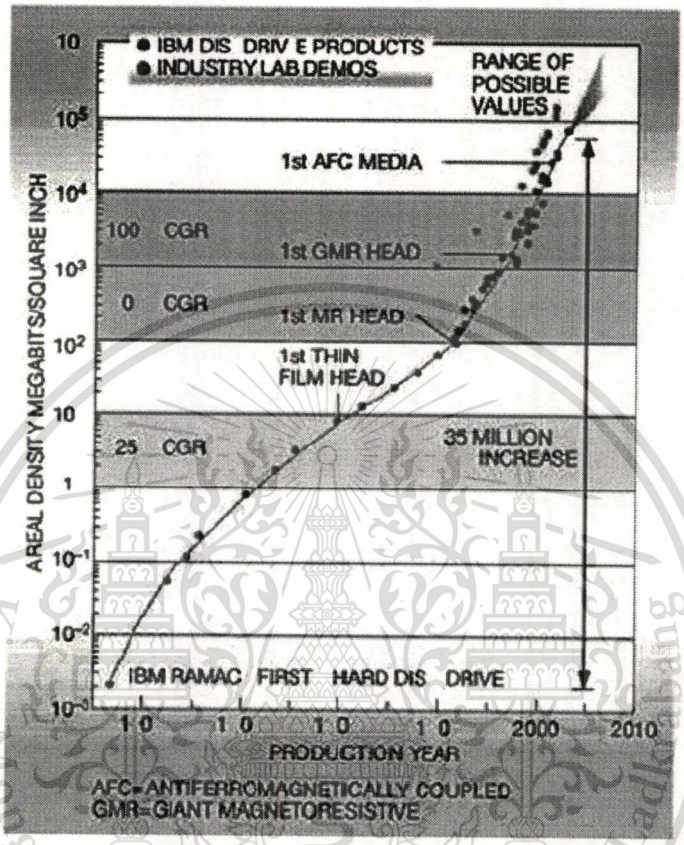

Figure 1.1 Trend in HDD areal density [24].

Ideally, in order to perform read/write head operation, the read/write head must be positioned within the boundary of ±10% of media track width all the times. In addition, the control technique must be robust for disturbance rejection and uncertainty. In HDD system, there are 2 types of external disturbance that could affect control system, repeatable run out (RRO) and non-repeatable run out (NRRO). RRO is a disturbance where its frequency is synchronous with the spindle rotation frequency, or one of its multiples. RRO is caused by sources like bearing geometry and motor geometry. In the other hand, NRRO sources are external disturbances which are not synchronous with the spindle rotation such as external shock, electrical noise or wind-induced vibration. In generals, the RRO magnitude is higher than that of NRRO [4]. In order to achieve higher areal density, servo mechanical control should be able to get rid these disturbances, and keep the head staying in the middle of the media track.

1.3 Objectives

The objectives of this thesis are as following.

- To study dual-stage actuator plant system identification.
- To study and compare the performance of the quantitative feedback theory and the controller conventional control technique.

1.4 Thesis Scope

The identification of the dual-stage actuator plant would be done on frequency domain. The decoupling technique would be implemented to separate the servo loops of VCM actuator and micro actuator. The dual-stage actuator controller design must be able to meet the following performance criteria.

- The overshoot of the actual displacement must be less than 5%.
- The mean of the steady-state error must be zero.
- The gain and phase margins must be greater than 6dB and 30°.
- The maximum peaks of the sensitivity must be less than 10dB.
- The settling time of the step response must be as short as possible.

1.5 Expectation

The mathematical identification plant of the dual-stage actuator is expected as one of the results of this study. The mathematical model would be verified with actual drives by comparing the positioning signal errors of the actual experimental signals and the calculated ones. Another result is the implementation of QFT as the controller to the dual-stage actuator.

MatLab program would be used throughout the research study from the system identification, controller design to the controller performance simulation. This thesis has been using QFT toolbox of "Terasoft company" (www.terasoft.com) MatLab tools box to design the QFT controller and fine tune for disturbance rejection.

1.6 Conceptual Framework

Plant identification would be done on frequency response. Sweep sine commands would be fed to the actual dual-stage actuator. The actuator output would be collected to obtain the plant transfer function.

Only computer simulation would be done to investigate the ability of the proposed QFT controller. Due to RRO magnitude and its affect are higher than

those, only RRO would be used as disturbance into the plant with the purposed QFT controller technique. The closed loop performance of QFT controller would then be compared with that of conventional PID controller.

1.7 Hypothesis

Increasing of areal density could be done by increasing the number of track. In order that the size of media remains unchanged, the track pitch must be smaller. If the QFT controller could reject the disturbance and minimize the head vibration, the track pitch could then be smaller, hence the areal density could be increased.

1.8 Thesis Outline

The remaining of thesis outlines are as below following:

Chapter2. This chapter presents backgrounds in the single-stage and dual-stage actuator, run out issue in hard drives, and system identification. It also reviews general controller theories, quantitative feedback theory and some other methods in the literature.

Chapter3. This chapter presents conventional control methods used and their concerns. The dual-stage actuator system identification in frequency domain would be explained and its frequency response would be obtained. The application of the notch filter to suit for uncertainty plant of VCM and PZT is also explained. The disturbance model is presented. The disturbance model would be input into the dual-stage actuator model for verification of the system identification. The precision of system identification would be confirmed by positioning error signals from the model with the experimental actual ones. The peak to peak amplitude of positioning error signals is the criterion of the system identification precision. This chapter will also introduce the decoupling technique which would be implemented to the dual-stage actuator.

Chapter4. This chapter presents the design of quantitative feedback theory (QFT). There are three steps for tuning the controller. First, the plant template plot is done on Nichols chart. Then the allowable region is identified. All of them will be add into the Nichols chart for the controller loop shaping, include the pre-filter loop shaping. The simulation results would be shown at the end of this chapter.

Chapter5. The conclusion is stated in this chapter.

CHAPTER 2
LITERATURE REVIEWS

2.1 Frequency domain system identification

Al Manum et al. [1] presented the system identification of a VCM actuator. Figure 2.1 shows the block diagram of the experimental setup used in the study. The motion of the actuator sensed by the Laser Doppler Vibrometer (LDV) was fed to Digital Signal Analyzer (DSA). DSA also generated command signal to VCM driver to drive VCM.

System identification was done on frequency domain. The math model was obtained by least-square fit of the actual frequency response of the VCM actuator.

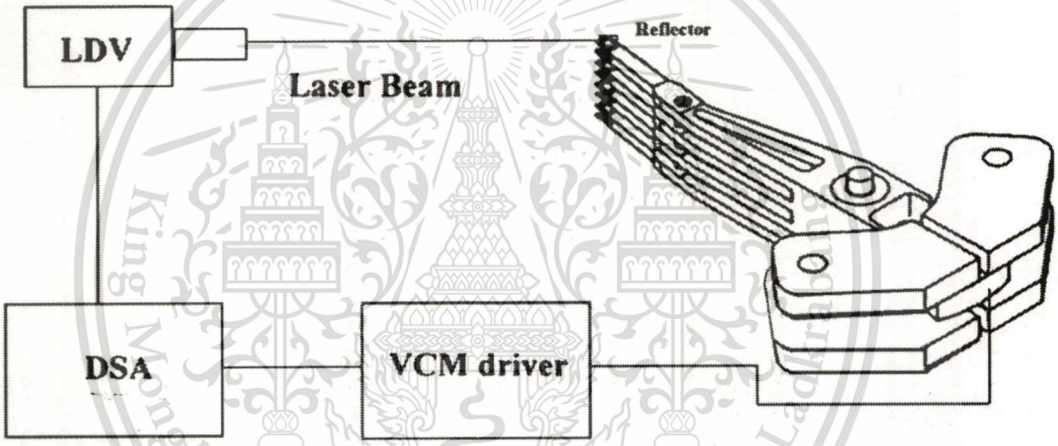

Figure 2.1 Experimental setup for frequency response measurement [1].

Nagashima and Nakagawa [20] presented the design of a multi-rate filter in order to attenuate the resonances above the niquist frequency. The study showed that the controller design would be less complex after implementation the multi-rate filter.

2.2 Dual-Stage Actuator(DSA)

DSA was proved to be able to increase system bandwidth and disturbance to system, thus it can also improve track following performance. Peng et al.[4] presented a dual-stage actuator that was able to improve the track following performance compared with a single-stage actuator. The dual-stage controller was based on composite nonlinear control approach for track seeking, and achieved the following performance criteria.

- The control input to the VCM actuator should not exceed ±3 V, where as the control input to the micro-actuator should be within ±2 V.
- The displacement of the micro-actuator should not exceed $1\mu m$. Moreover, it should settle down to zero in the steady state so that the micro-actuator can be further used for the next motion.
- The overshoot and undershoot of the step response should be kept less than 0.05 μm, i.e., 5% of one track pitch. The R/W head of the HDD servo system should start reading or writing data on to the disk within 5% of one track pitch of the target.
- The gain margin result should be larger than 6 dB and the phase margin should be more than 50°.

The tables 2.1 and 2.2 show the performance comparison of the single-stage and dual-stage actuator. It shows that the dual-stage actuator had better performance and less error. Figure 2.2 shows RRO disturbance rejections of both single-stage and dual-stage actuator.

Performances of single- and dual-stage HDD servo systems

Target (μm)	Single	Dual	Improvement (%)
Panel A: Simulation results: settling time (ms)			
1	1.85	0.95	49
20	3.10	2.70	13
50	3.60	3.20	11
Panel B: Experimental results: settling time (ms)			
1	1.9	1.0	47
20	6.5	5.3	18
50	8.2	6.2	24

Table 2.1 The performances comparison of single-stage and dual-stage actuator [4].

	Single	Dual	Improvement (%)
$3\sigma_{pes}$ (μm)	0.049	0.030	39

Table 2.2 The $3\sigma_{PES}$ performances of single-stage and dual-stage actuator [4].

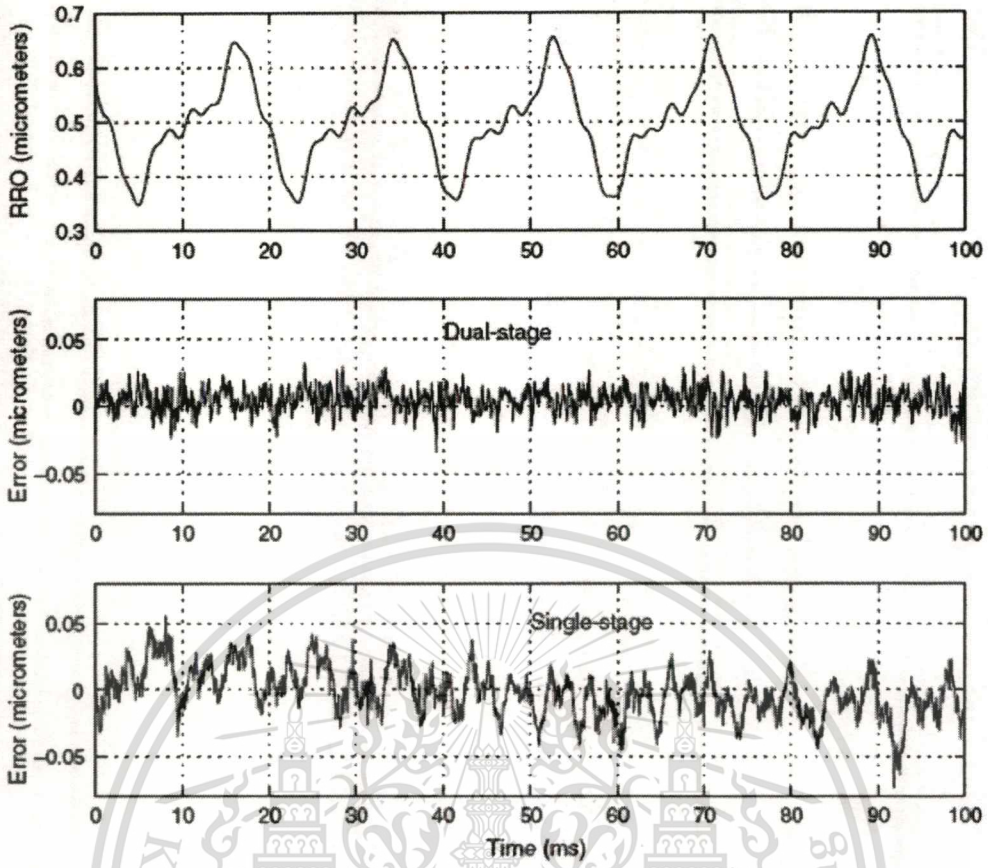

Figure 2.2 Performance of disturbance rejection comparison between single-stage and dual-stage actuator [4].

Numasato and Tomizuka [3] presented a settling control of a dual-stage actuator system for hard disk drives. The decoupling filter, which was placed between the voice-coil motor (VCM) controller input and the PZT controller output, was a PZT output estimator so that the PZT actuator output was canceled out from the VCM controller input. Table 2.3 shows the experimental results of the dual-stage actuator. The dual-stage actuator had a better settling response than the single-stage actuator by 50%.

Description	Single-actuator	Dual-actuator
Settling response with $T_f = 15T_s$		
Settling error ($6E_s$)	$0.44\mu m$	$0.21\mu m$
Improvement	-	53%
Settling response with $T_f = 10T_s$		
Settling error ($6E_s$)	$0.57\mu m$	$0.27\mu m$
Improvement	-	53%
Settling response under vibration		
Settling error ($6E_s$)	$0.71\mu m$	$0.29\mu m$
Improvement	-	60%

Table 2.3 The settling time performances of single-stage and dual-stage actuator [3].

2.3 Dual-stage actuator with decoupling method

Horowitz et al. [21] presented the dual-stage servo systems and vibration compensation in HDD. They showed that the dual-stage actuator could increase higher bandwidth and improve the track-following capability of read/write head positioning control system.

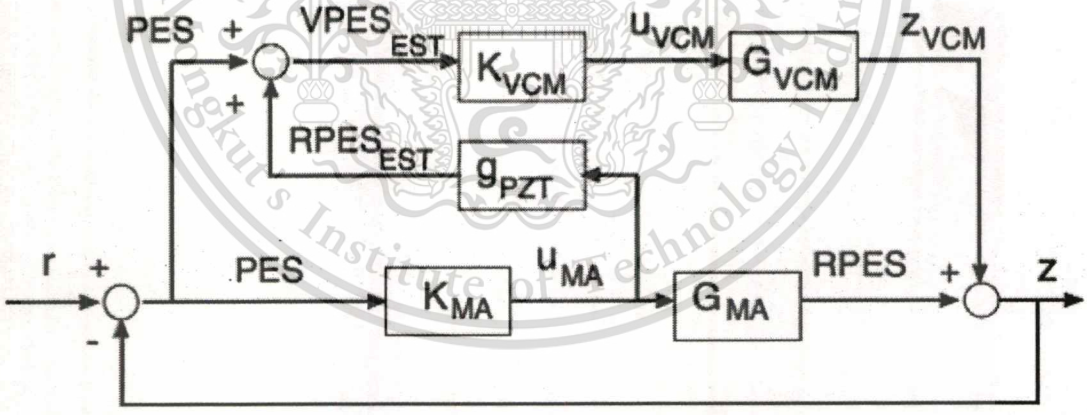

Figure 2.3 Block diagram of the track-following controller design using the sensitivity decoupling method [21].

The block diagram of the control system in the study [21] is shown in figure 2.3. The components of the block diagram are as follow:

- G_{MA} is the transfer function of the PZT-actuated suspension,
- G_{VCM} is the transfer function of the VCM-actuated suspension,
- K_{MA} is the PZT loop controller,

- K_{VCM} is the VCM loop controller,
- g_{PZT} is the decoupling loop controller.

The signals according to the diagram are:

- r is the track runout,
- z is the position of read/ write head,
- z_{VCM} is the position of suspension tip,
- PES is the position error between the head and the center of the track,
- $RPES$ is the position of the MA, which equal z-z_{VCM},
- U_{VCM} is the control input of VCM,
- U_{MA} is the control input of MA,
- $VPES$ is the position error signal between PES +$RPES$, which equal r - z_{VCM}.

Assuming that the relative position error signal ($RPES$) is equal to the position error signal estimate ($RPES_{EST}$), the closed-loop sensitivity transfer function $S_T(Z)$ is shown below.

$$S_T(Z) = \underbrace{\frac{1}{1+K_{VCM}(z)G_{VCM}(z)}}_{S_{VCM}(z)} \underbrace{\frac{1}{1+K_{MA}(z)G_{MA}(z)}}_{S_{MA}(z)} \tag{2.1}$$

Thus, the dual-stage servo control can be shaping-design individually and decoupled into two independent SISO sensitivity functions and is shown figure 2.4.

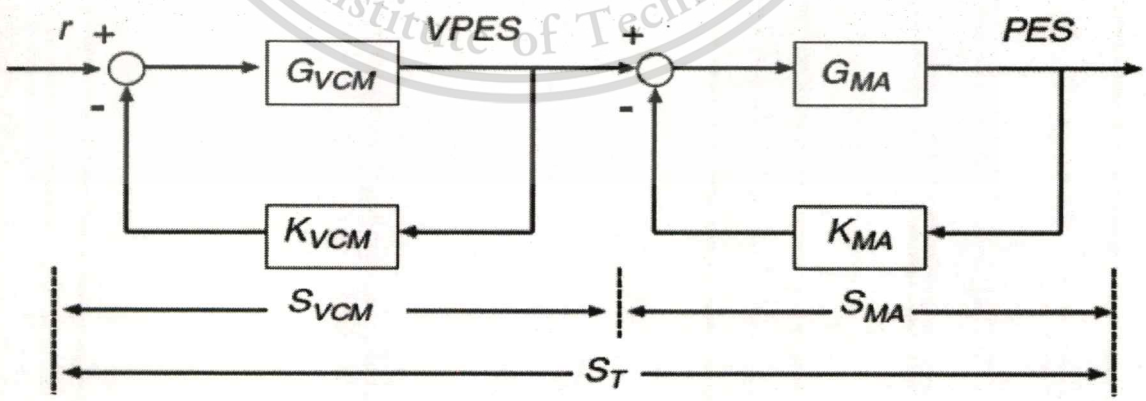

Figure 2.4 The equivalent blocks diagram uses for designing controller and controller with decoupling controller [21].

2.4 Conventional servo controller technique

Vagia and Nikolakannan [6] presented the Design of a robust PID-controller switching scheme for electrostatic micro-actuator. A robust switching PID controller coupled to a feed forward controller is designed for set-point regulation of the actuator. The nonlinear model of actuator is linearized at multiple operating points at which multiple PID controllers are designed (figure 2.5).

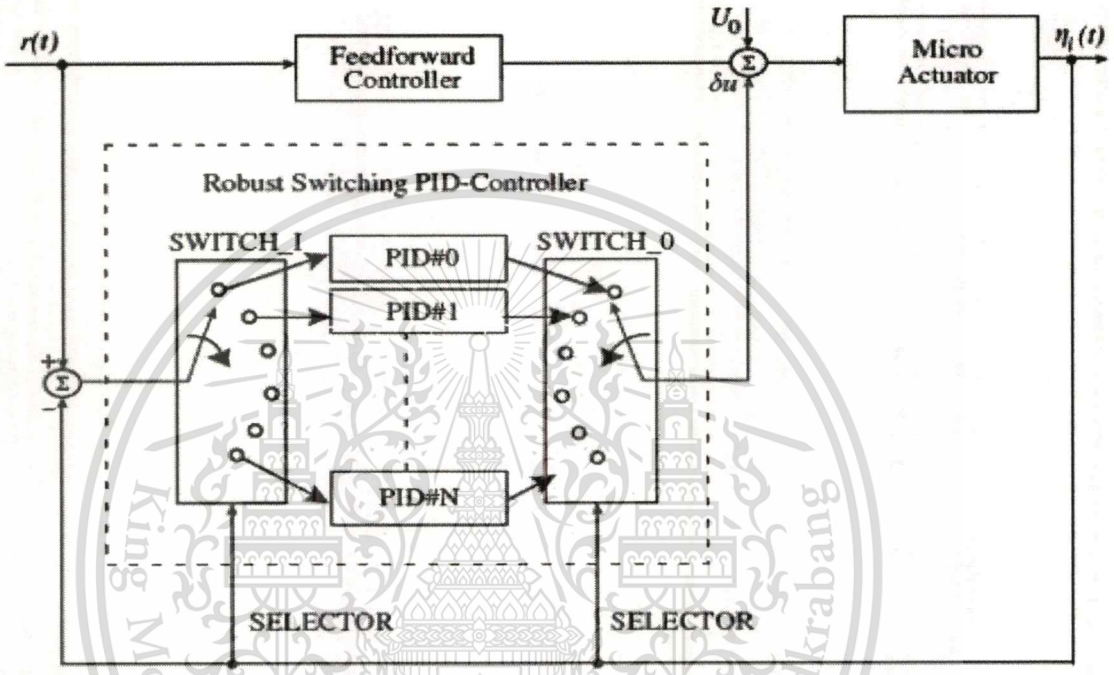

Figure 2.5 Feed forward and switching PID-control architecture [6].

Taghirad and Jamei [15] applied an adaptive robust control, originated by Yao (1997), to a hard disk drive. Zheng and Tomizuka[18] proposed an adaptive compensation scheme to estimate and compensate the dominant frequency component in the NRRO. Most of the adaptive algorithms are computationally intensive and have not yet been proven their practicality on experiments.

Du et al. [9] devised a linear controller based on solving linear matrix inequalities, a method proposed by Boyd et al. (1994), for actuator positioning. The disturbance was rejected using an adaptive nonlinear compensation. You and Hong [17] proposed a robust sliding mode control with a new switching surface for track following. Low and Wong [12] used multi-objective genetic algorithm in a controller-tuning scheme for a hard disk drive servo system by placing constraint objectives at higher priority than the optimization objectives. Park et al. [14] presented a hard disk

drive servo control based on repetitive control algorithm, proposed by Hara et al. (1988.).

2.5 Quantitative feedback theory (QFT)

The QFT was introduced by Horowitz [10] in 1959. Model uncertainties are considered explicitly during the control design process. Other specifications such as disturbance rejection, tracking, and stability can be specified to ensure that the control performance meets or exceeds these requirements.

Kyoung and Nguyen [19], Applied the QFT with hydraulic system which combines electric and electrohydraulic system, which was called a hybrid actuator system. Figure 2.6 shows the diagram of mini motion package (MMP) applied in robotic, automation, plastic injection-modeling and metal forming technology.

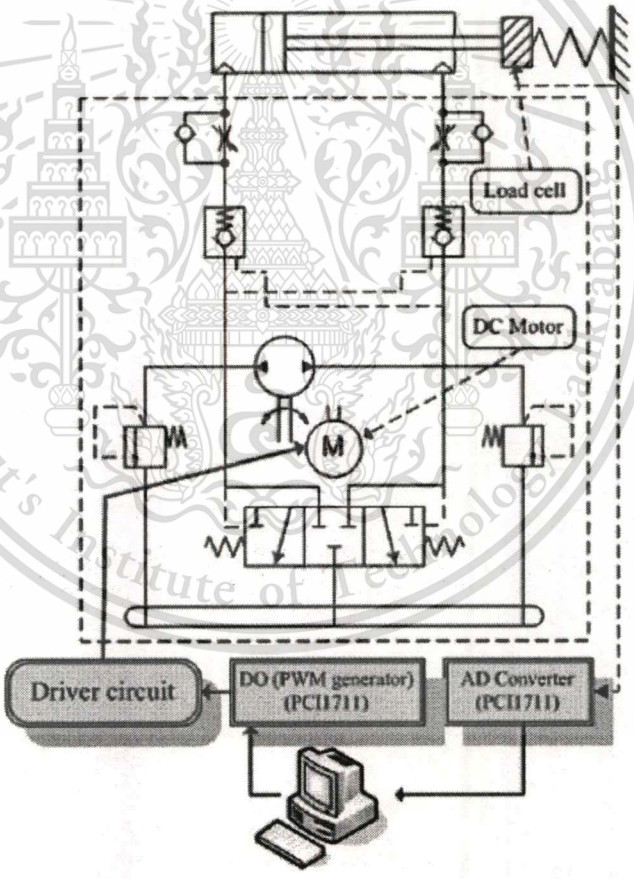

Figure 2.6 Schematic diagram of MMP [19].

QFT the block diagram of controller used in [19] is shown in figure 2.7. The QFT controller gave more robust force tracking performance compared with PID

controller. Good performance could be achieved even though the stiffness of environment and set-point force were changed.

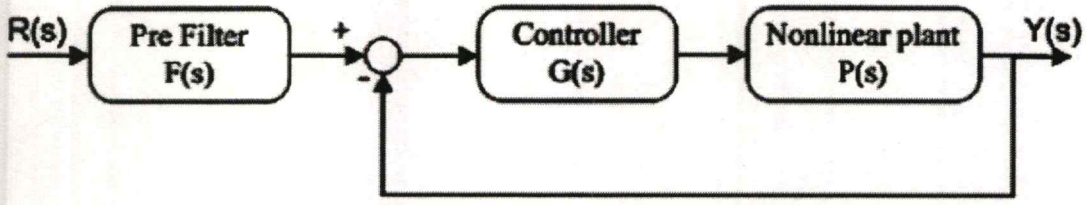

Figure 2.7 Structure of QFT control diagram [19].

Zhang et al. [8] applied QFT to permanent magnet linear motor (PMLM) to control the position with cogging force compensation at high acceleration rates. Figure 2.8 shows the schematic drawing of the linear positioning stage used in the study. A PMLM was mainly composed of the two parts, a stator and a mover. The mover hosted a three- phase winding generating a magnetic field following along the linear axis. The stator was made from series of permanence magnets.

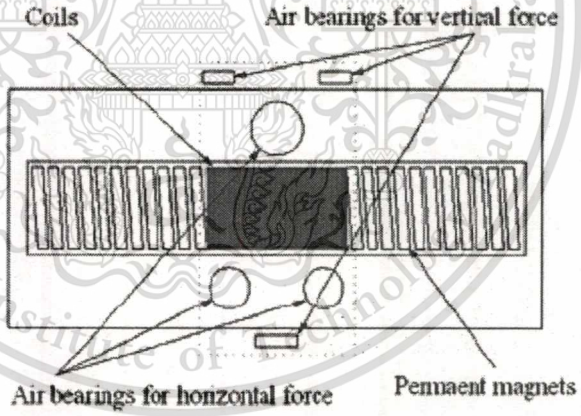

Figure 2.8 Drawing linear positioning stage [8].

Figure 2.9 shows frequency response of the positioning stage, which was a double integrator and at high frequency had some the resonances. The cogging force of a PMLM was the normal force produced by the interaction between the teeth of the mover and the edges of the permanent magnetic of the stator. Figure 2.10 shows the experimental results which demonstrated the feasibility and effectiveness of the proposed method.

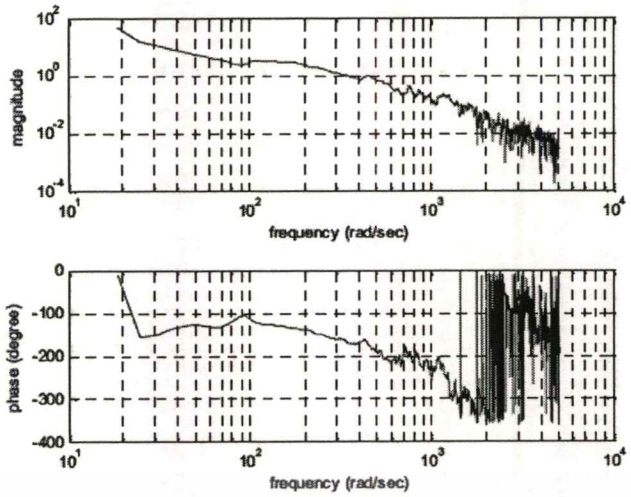

Figure 2.9 Frequency response of the linear positioning stage [8].

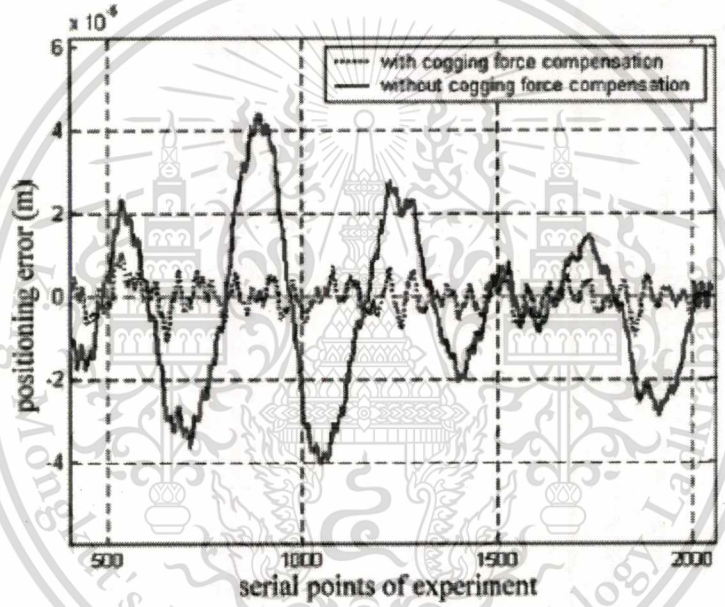

Figure 2.10 Comparison of tracking errors with and without controller [8].

2.6 Summary of literature reviews

- The literature reviews show that the dual-stage actuator could increased the open loop bandwidth [4] compared with the single-stage actuator. This could improve the performance of track following and reduce the settling time [3].
- The challenge of the implementation of the dual-stage actuator into hard disk drives is how to control VCM and PZT loop simultaneously. The master – slave decoupling method [21] is one way to control the individual plants of VCM and PZT to simultaneously by adding one controller gain between VCM and PZT loop.

- The present of conventional controller is PID controller [6] which achieve the current head positioning accuracy demand would be a bottom neck in the developing process of large capacity in HDDs.
- The QFT controller is a potential controller due to its better robustness than the conventional PID controller [19]. QFT was successfully applied to a permanent magnet linear motor (PMLM) [8]. The identification of PMLM model is a second order type which similar to the VCM actuator plant. The following performance of QFT controller was shown to be better than the PID controller [8]. The QFT controller is then proposed to be the controller with dual-stage actuator in this thesis study.

CHAPTER 3

Dual-Stage Actuator modeling

3.1 Modeling of a Dual-stage actuator

The schematic drawing of a dual-stage actuator used in this thesis study is shown in figure 3.1. The structure of a dual-stage actuator is the same as a VCM actuator but mounted on top by a piezoelectric transducer (PZT) actuator. The VCM is used for generating the magnetic force to move the arm in the concentric rotation, where a pivot bearing would be fixed at the concentric rotation center. At the end of the VCM arm, a PZT is mounted. The PZT will move as the second actuator. The read/write head is installed at the end of the extended PZT arm. The head is used for reading and writing the data.

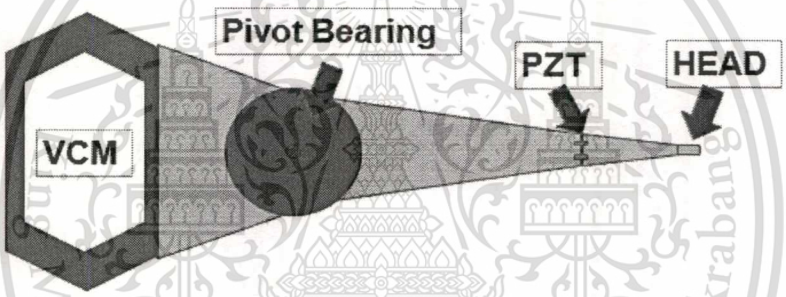

Figure 3.1 Drawing of a VCM with amounted PZT

The frequency responses of VCM and PZT are measured by displacement of head when the system is injected by sweep sine command signals.

$$G = \frac{\omega_p^2}{S^2+2\xi\omega_p S+\omega_p^2} \tag{3.1}$$

$$Resonance\ mode = \prod_{i=1}^{n} \frac{S+2\xi_{zi}\omega_{zi}S+\omega_{zi}^2}{S+2\xi_{pi}\omega_{pi}S+\omega_{pi}^2} \tag{3.2}$$

ω_{pi} is the rotating speed of pole
ω_{zi} is the rotating speed of zero
ξ_{pi} is the damping factor of pole
ξ_{zi} is the damping factor of zero

The transfer function of VCM and PZT can be obtained by combining all the resonance modes represent in equation 3.2. Each resonance mode is modeled as a second order resonance in equation 3.1.

However, phase and gain distortion due to the actuator resonances would affect the overall phase and gain margins. This problem has been fixed by using a pre-controller in flexible modes which the possible way to fix is as the gain stabilization. A notch filter is a typical gain stabilization method to suppress the structural resonances. Application of notch filter for gain stabilization is illustrated in this section by using a plant model which contains only one lightly damped resonance mode, and this idea could be applicable to actuators with multiple flexible modes.

The model of VCM and PZT would include notch filler to attenuate resonance frequency in order to stabilize the system. The notch is represented by equation 3.3.

$$N(s) = \prod_{i=1}^{n} \left(\frac{\omega_{pi}^2}{\omega_{zi}^2}\right)\left(\frac{S+2\xi_{zi}\omega_{zi}S+\omega_{zi}^2}{S+2\xi_{pi}\omega_{pi}S+\omega_{pi}^2}\right) \tag{3.3}$$

The Bode plot of the open loop VCM actuator and PZT plant with and without notch filler show in figure 3.2 and figure 3.3 respectively. The solid line is the frequency response without notch filler. There are many resonance peak magnitudes that could be made the plant unstable easily. To fix it, the notch filler will be applied which show in dotted line. Many resonance peak magnitudes are able to be attenuated.

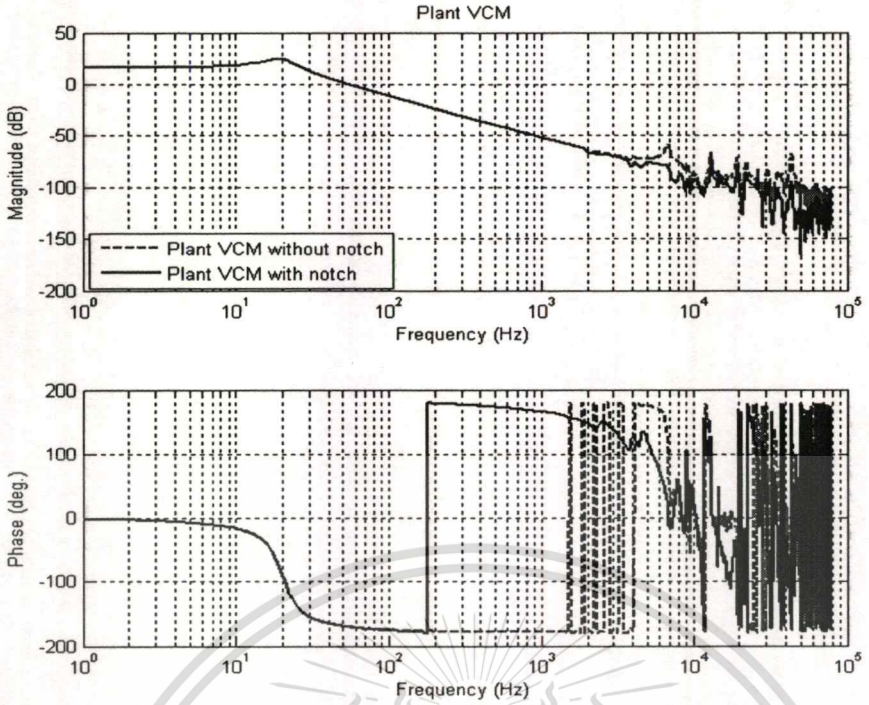

Figure 3.2 Frequency responses of the VCM with and without notch.

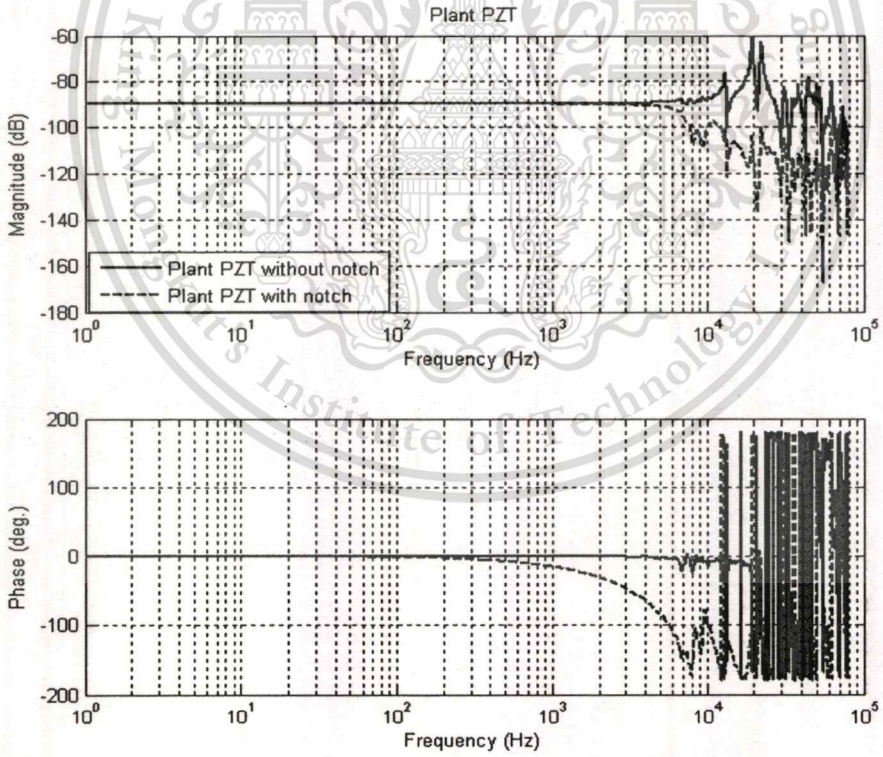

Figure 3.3 Frequency responses of the PZT with and without notch.

Figure 3.4 shows the VCM dynamic system after the identification. The Bode plot of frequency response will be used to design the controller. The dotted line is the actual VCM plant and the solid line is the plant fitting.

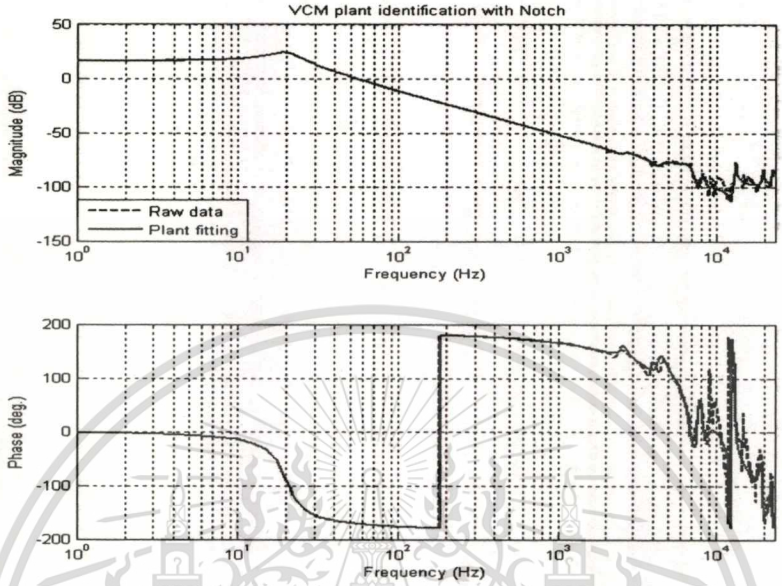

Figure 3.4 The estimated model of the VCM.

The VCM plant identified according to figure 3.4 contains 9 resonance modes referred in equations 3.4 to 3.12, where $G_{v,i}$ is the transfer function of resonance mode i.

$$G_{v,1} = \frac{2.406S+1.543x10^4}{S^2+49.83S+1.579x10^4} \quad (3.4)$$

$$G_{v,2} = \frac{S^2+2078S+2.57x10^8}{S^2+2314S+2.706x10^8} \quad (3.5)$$

$$G_{v,3} = \frac{S^2+3204S+7.43x10^8}{S^2+5322S+7.972x10^8} \quad (3.6)$$

$$G_{v,4} = \frac{S^2+2617S+2.265x10^9}{S^2+6006S+1.82x10^9} \quad (3.7)$$

$$G_{v,5} = \frac{S^2+6690S+2.847x10^9}{S^2+2653S+2.668x10^9} \quad (3.8)$$

$$G_{v,6} = \frac{S^2+2263S+6.111x10^9}{S^2+1364S+6.83x10^9} \quad (3.9)$$

$$G_{v,7} = \frac{S^2 - 7.238x10^4 S + 3.683x10^9}{S^2 + 9.338x10^4 S + 5.806x10^8} \quad (3.10)$$

$$G_{v,8} = \frac{S^2 + 1.048x10^4 S + 1.601x10^{10}}{S^2 + 1980x10^4 S + 1.498x10^{10}} \quad (3.11)$$

$$G_{v,9} = \frac{S^2 + 2.341x10^4 S + 1.809x10^{10}}{S^2 + 3935S + 1.974x10^{10}} \quad (3.12)$$

So the transfer function of VCM G_v can represented bellow.

$$G_v = G_{v,1}G_{v,2}G_{v,3}G_{v,4}G_{v,5}G_{v,6}G_{v,7}G_{v,8}G_{v,9} \quad (3.13)$$

The frequency responses of the PZT are shown in figure 3.5. The dotted line is the actual PZT plant and the solid line is the plant fitting.

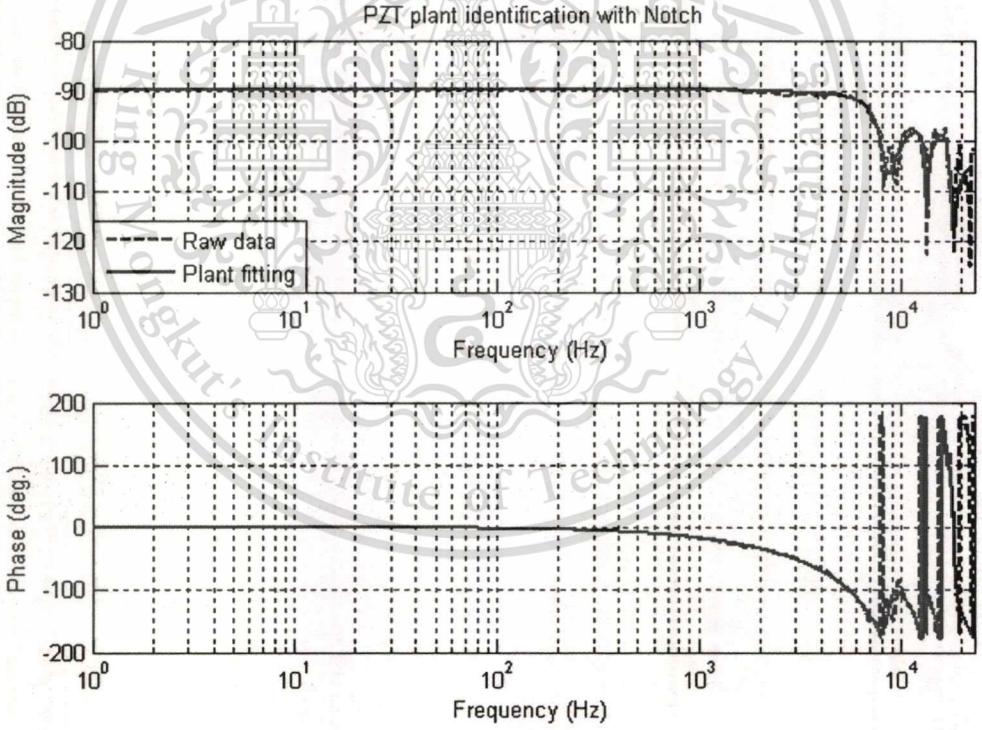

Figure 3.5 The estimation model of PZT with notch

The PZT plant identification according to figure 3.5 contain 5 resonance modes referred in equation 3.14 to 3.18, where $G_{p,i}$ is the transfer function of resonance mode i.

$$G_{p,1} = \frac{-1.696x10^{-9}S+1.039}{S^2+2.163x10^4S+2.336x10^9} \quad (3.14)$$

$$G_{p,2} = \frac{S^2+3896S+2.945x10^9}{S+4.459x10^4} \quad (3.15)$$

$$G_{p,3} = \frac{S^2-1423S+7.041x10^9}{S^2+9783S+6.734x10^9} \quad (3.16)$$

$$G_{p,4} = \frac{S^2-1.998x10^4S+1.2x10^{10}}{S^2+1.671x10^4S+1.14x10^{10}} \quad (3.17)$$

$$G_{p,5} = \frac{S^2+4045S+2.096x10^{10}}{S^2+4065S+2.096x10^{10}} \quad (3.18)$$

So the transfer function of PZT G_p can represented bellow.

$$G_p = G_{p,1}G_{p,2}G_{p,3}G_{p,4}G_{p,5} \quad (3.19)$$

3.2 Plant Verification

The mathematical models obtained in the topic 3.1 can be verified by comparing position error signal between actual measured singnal and simulation data based on plant mathematical model. The actual measurement is taken on bench HDD by monitoring positioning signal error (PES) from read back signal. This data has shown total run out (TRO) or track mis-registration (TMR) which consists of repeatable run out (RRO) and non-repeatable run out (NRO). The RRO signal in real drives are composed mostly of sinusoidal wave and its magnitude is much larger than that of NRO [4]. Only RRO disturbance source will be used in this thesis study. Figure 3.6 shows the RRO signal recorded from the actual HDD implementation. Figure 3.6(a) shows the time trace of RRO, and figure 3.6(b) shows its spectrum which consists of many harmonics. The harmonic with magnitude of at least 4 nm are considered to be dominant in this study. There are total of 6 dominant harmonics (1x,2x,3x,65x,67x, and 71x) that can be expressed as a Fourier series as shown in equation 3.20.

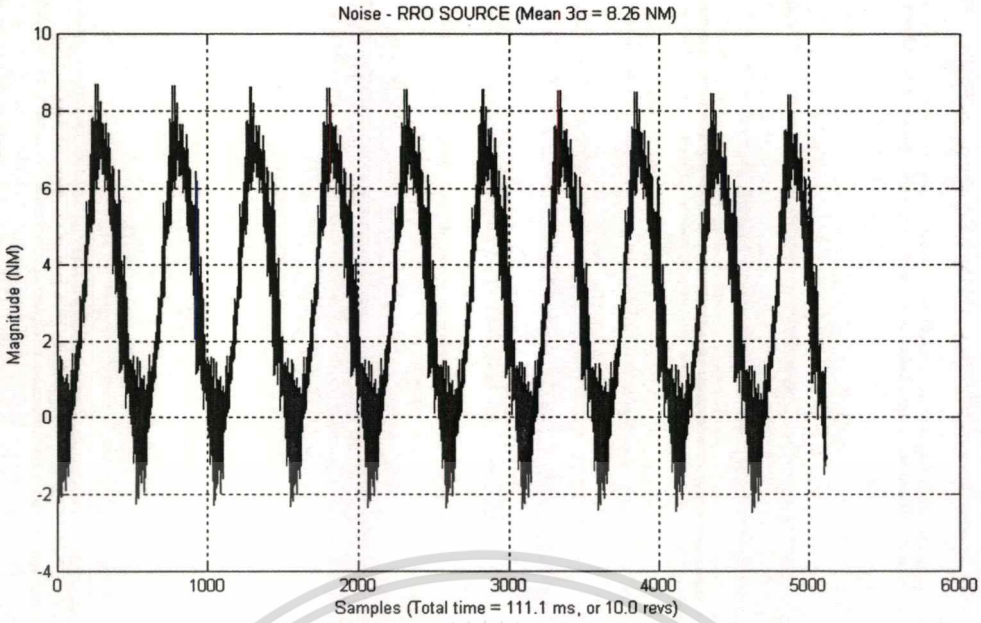

(a)

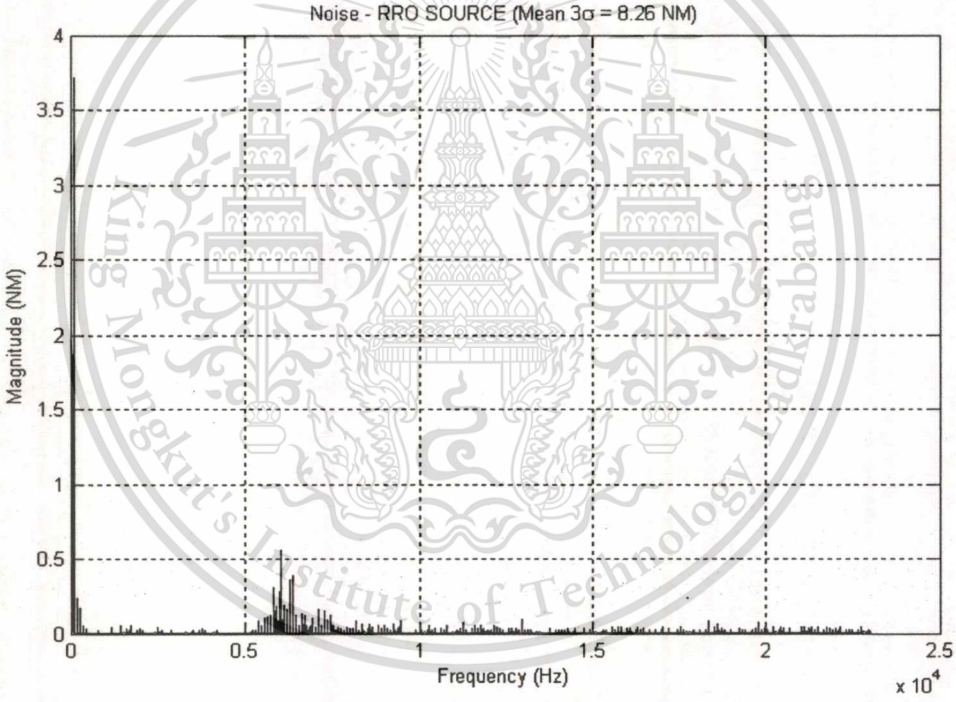

(b)

Figure 3.6 RRO disturbance from bench measurement
(a) RRO disturbance in time domain,
(b) RRO disturbance in frequency domain.

Approximated RRO disturbance from PES could be represented by mathematic estimation model from spectrum frequency in equation below.

$$tmr = 3 + 3.72\cos(2\pi\omega t) + 0.243\sin(2\pi 2\omega t) + 0.1754\sin(2\pi 3\omega t) + 0.3\sin(2\pi 65\omega t) + 0.5574\sin(2\pi 67\omega t) + 0.5574\sin(2\pi 71\omega t) \quad (3.20)$$

The time trace of the RRO disturbance model from equation 3.20 is shown in figure 3.7.

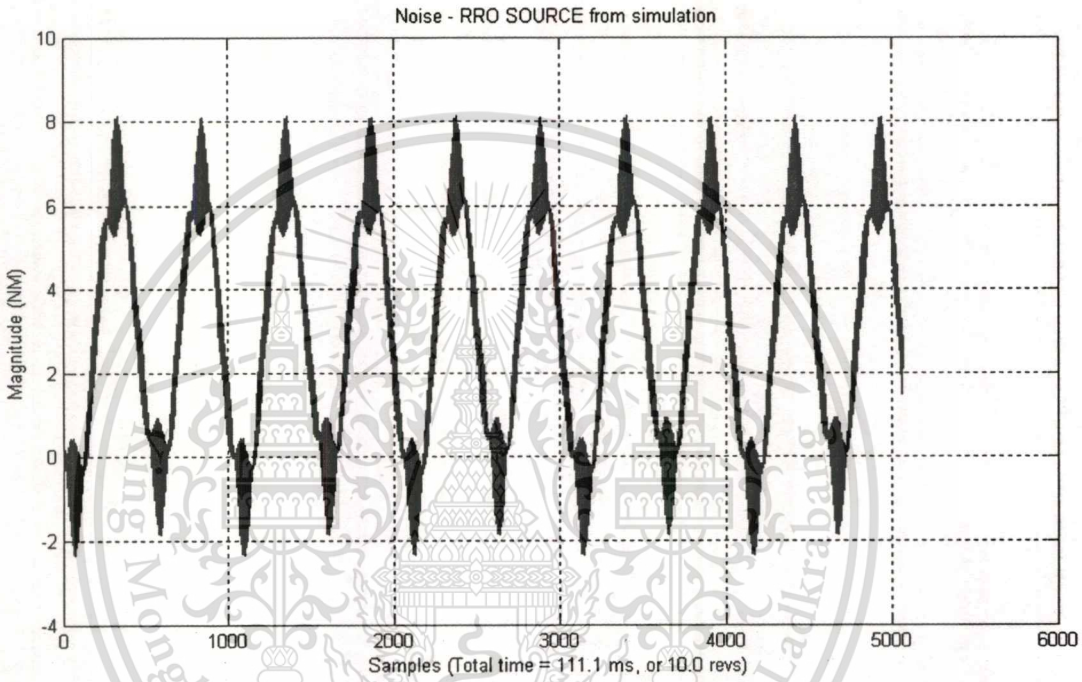

Figure 3.7 Estimated RRO disturbance.

The comparison of the actual and the modeling RRO disturbance is shown in figure 3.8. The solid line is the disturbance RRO which is real measurement from the HDD drives and dotted line is the modeling disturbance RRO (equation 3.20).

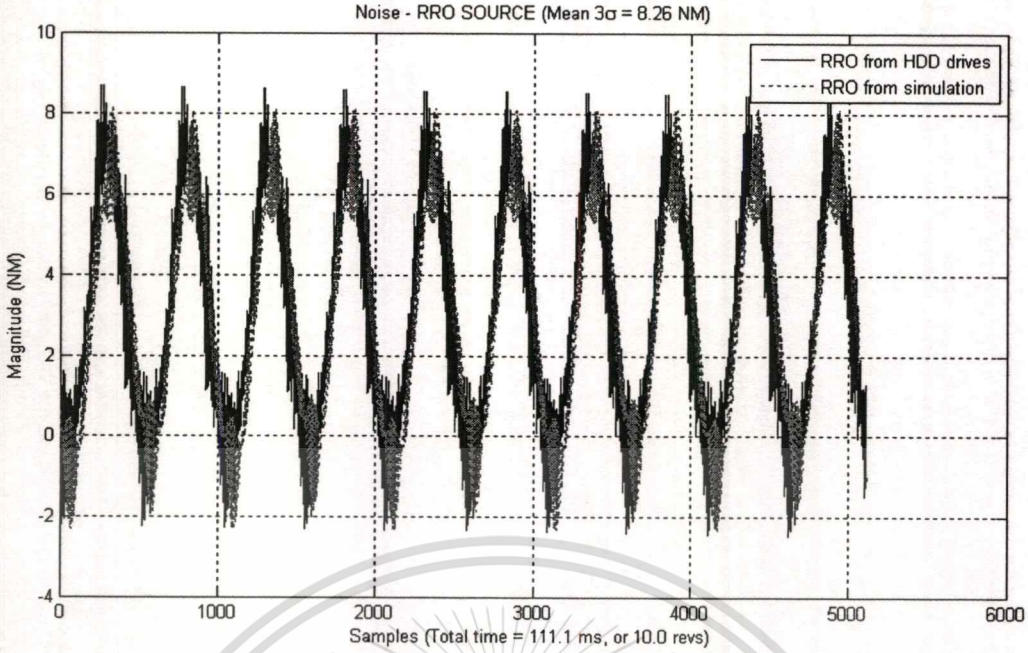

Figure 3.8 RRO comparison between measurement and simulation.

Figure 3.9 shows the spectrum of the difference between actual RRO from actual HDD and estimated RRO (equation 3.20).

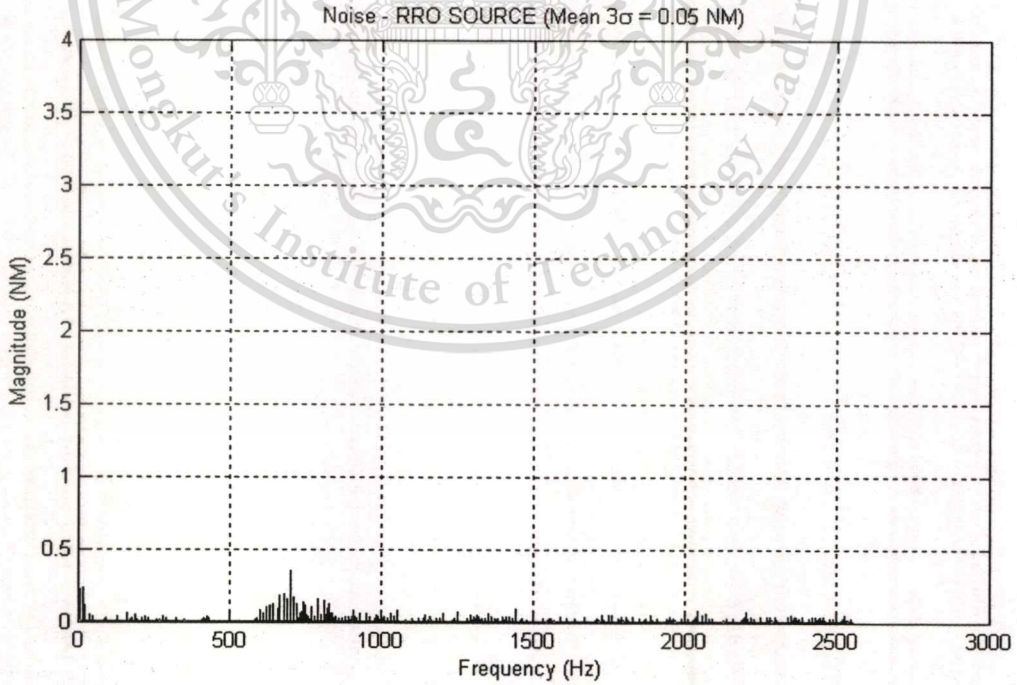

Figure 3.9 The spectrum difference between actual RRO and estimated RRO.

The RRO disturbance mode will be substituted into the servo loop system. The verification of system identification is done by monitoring from positioning error signal (PES) amplitude. The figure 3.10 shows the comparison between actual positioning error signal (PES) and the results from simulation of the plant model. The simulation results of the plant model are comparable with the actual signal as can be seem from the similar magnitudes and frequencies of both signals.

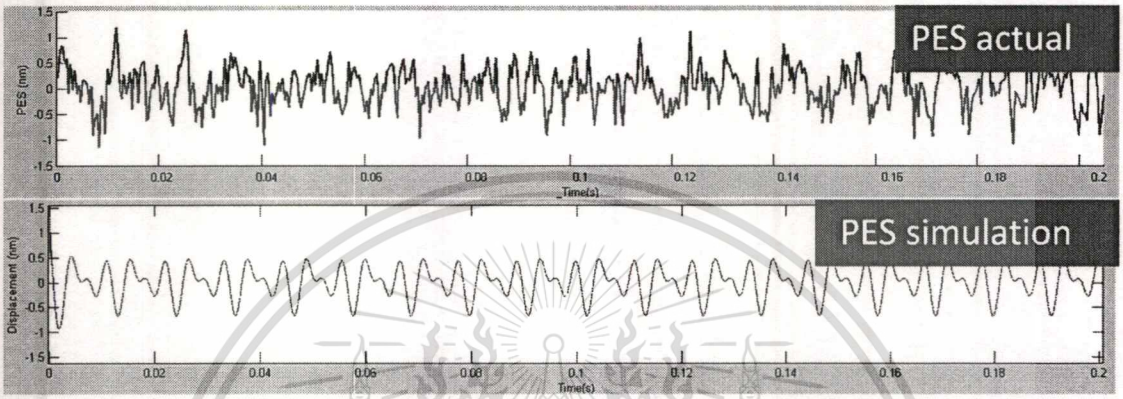

Figure 3.10 PES comparison between actual measurement and simulation.

3.3 Disturbance modeling

The diagram of read/write head positioning servo-mechanism is shown in figure 3.11. The read positioning data, read by head, is fed to PES Demonstrator (PES Demon) to convert to PES signal. The PES signal is then fed to servo processer. The servo processer calculates the actuator drive signals according the feedback PES signal. Output from servo processer is amplified by the VCM driver, and then is fed to drives both VCM and PZT actuators. In the actual HDD, the dual-stage actuator plant are under various disturbances, ie: external vibration, air turbulence, transient vibration, bearing run out, media noise, media defects, and PES nonlinearity. All of them effect off-track of the read/write head.

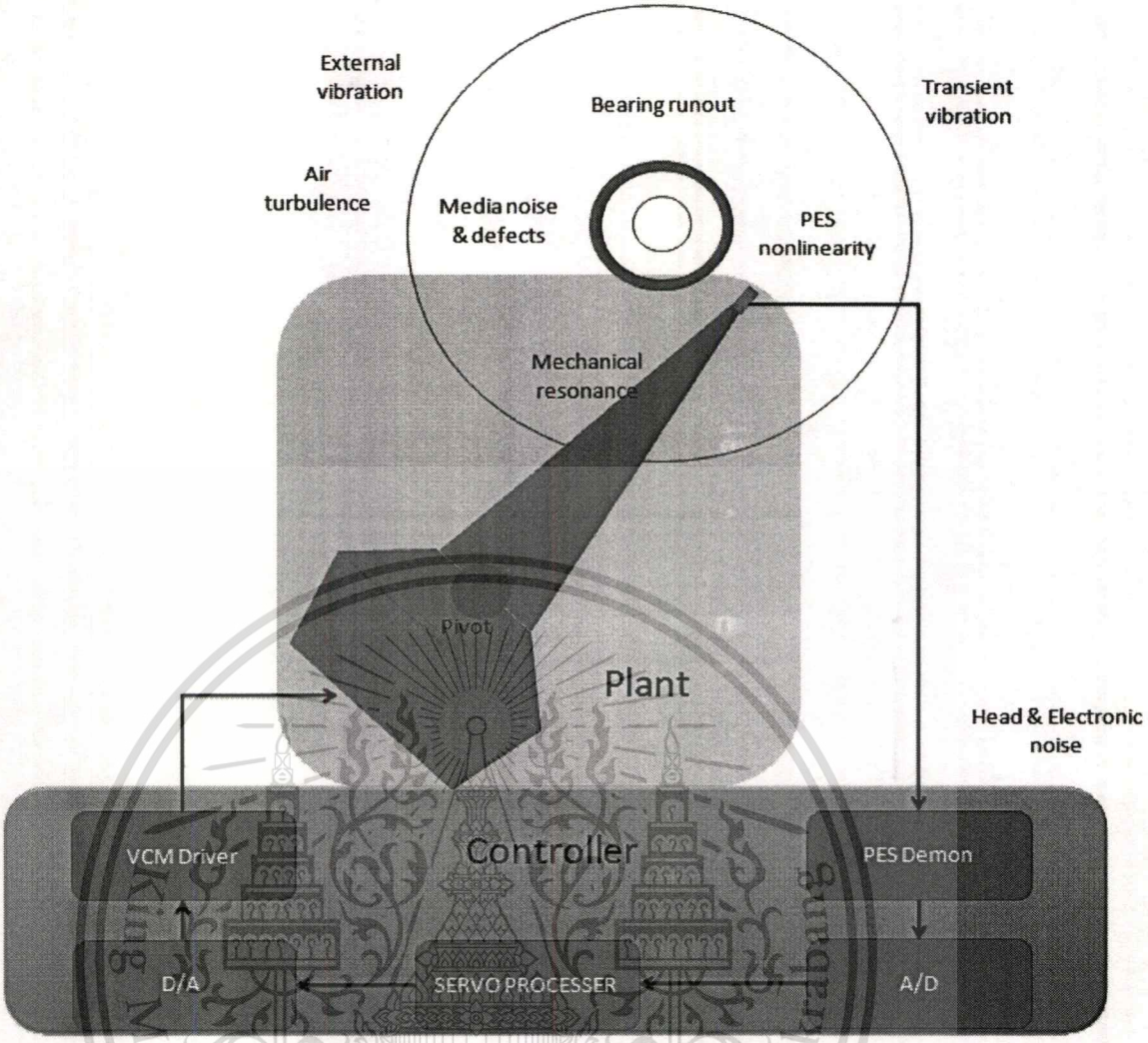

Figure 3.11 Disturbance model diagram.

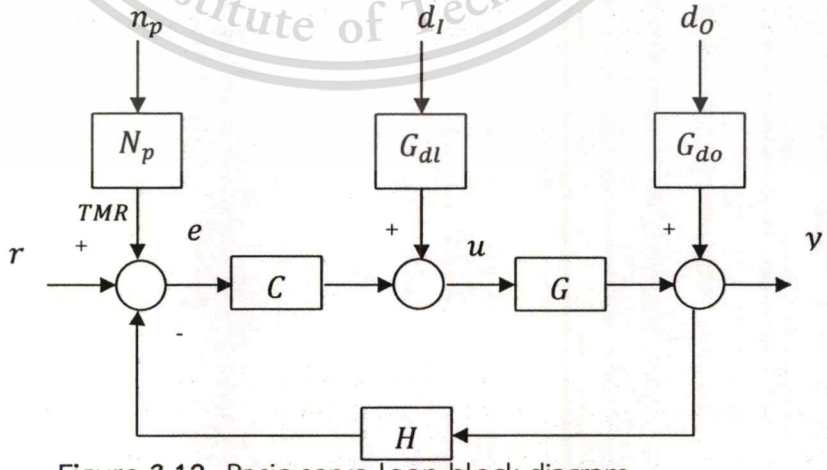

Figure 3.12 Basic servo loop block diagram.

The block diagram of basic servo loop is shown in figure 3.12. The function of each block is defined as follows.

- G the is plant transfer function, which includes all possible of variation due to uncertainties in a set $\{G\}$. For the VCM actuator, G is represented by G_v according to equation 3.13. For the PZT actuator, G is represented by G_p which is equation 3.14.
- H is the sensor transfer function, which is considered to be unity in this thesis study.
- C is the controller transfer function. For the VCM actuator, C is represented by C_v, and for the PZT actuator, C is represented C_p,
- N_p is the noise transfer function,
- $G_{dI}$is the transfer function of input disturbance,
- G_{do} is the transfer function of output disturbance.

The signals in the block diagram (figure 3.12) are defined as follow.

- n_p is the noise source.
- r is the reference input for track following, a zero value, meaning that the head stay in the middle of the track.
- e is the positioning error signal.
- u is the control output.
- y is the plant output.
- $d_I$is the input disturbance,
- $d_O$is the output disturbance.

The signal could be written in the frequency domain (S-domain) as

- $e = E(s)$,
- $u = U(s)$,
- $y = Y(s)$,
- $r = R(s)$.

In actual HDD implementation, the output signal is not measured directly. The positioning error e is measured instead.

$$E(s) = \frac{1}{1+CP}[R + Np - G_{dI}G + G_{do}] \tag{3.21}$$

So sensitivity function is

$$S(s) = \frac{1}{1+CP} \tag{3.22}$$

Equation 3.21 could be rewritten as equation 3.23.

$$E(s) = S(s)[R + Np - G_{dI}G + G_{do}] \tag{3.23}$$

The TMR or track mis-registration is overall disturbance and noise which disturb read/write head to be off track, and could be explained as equation 3.24.

$$TMR(s) = [R + Np - G_{dI}G + G_{do}], \tag{3.24}$$

Therefore, error could be described by TMR as

$$E(s) = S(s)TMR(s) \tag{3.25}$$

3.4 Control of Dual-Stage Actuator with Decoupled Master-Slave (DMS)

The dual-stage control system is the multi-input multi-output (MIMO) control system type as the servo loop of both the VCM actuator and PZT actuator are dependent to each other. The decoupling master-slave (DMS) has been previously implemented successfully to the dual-stage actuator [21]. With DMS, the controller of each actuator could be designed independently.

The block diagram of DMS controller system used in this thesis study based on [21], is shown in figure 3.13.

- G_v is the VCM plant (equation 3.13).
- N_v is the notch filler (equation 3.3) to stabilize the system.
- C_v is the VCM controller.
- $G_p$is the PZT plant (equation 3.19).
- N_p is the notch filler for PZT plant (equation 3.3).
- C_p is the PZT plant controller.
- $\hat{G}_p$is the decoupling filter placed between VCM controller input and the PZT controller output. It can be thought as the PZT output estimator. With $\hat{G}_p$, PZT actuator output is cancelled at the VCM controller input.

The signals in the block diagram (figure 3.13) are defined as follow.

- P_{ref} is input command for DSA actuator movement which it is assumed to be a zero during track following, demanding the head to stay in the middle of the track.
- Track Mis-Registration (***TMR***) is the disturbance source which consists of RRO components as shown in equation 3.20.
- ***PES*** is the positioning error signal which is the controller input.

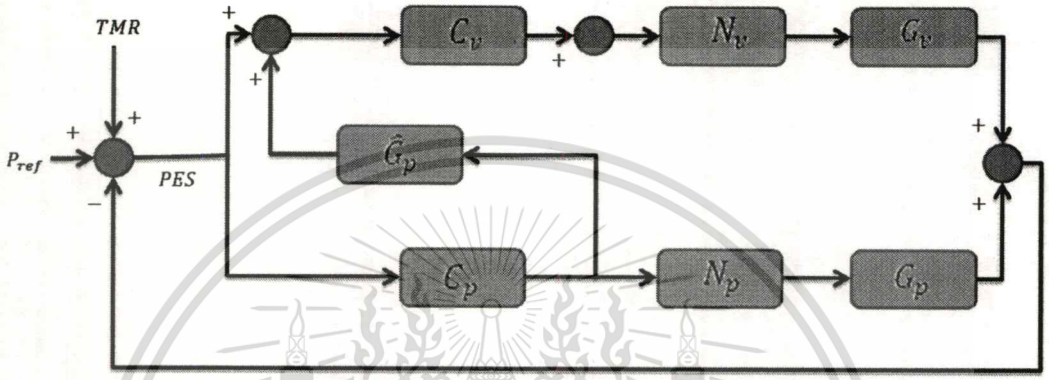

Figure 3.13 The block diagram of dual-stage actuator.

From block diagram, the open loop gain could be represented by equation 3.26.

$$G_o(s) = C_v N_v G_v + C_p N_p G_p + C_p \hat{G}_p C_v N_v G_v \tag{3.26}$$

Assumed the decoupling $\hat{G}_p = N_p G_p$ then equation 3.26 can be rewritten as equation 3.27.

$$G_o(s) = C_v N_v G_v (1 + C_p N_p G_p) + C_p N_p G_p \tag{3.27}$$

The sensitivity of the dual-stage actuator is shown in equation 3.28.

$$S(s) = \frac{1}{1+G_o} = \frac{1}{(1+C_v N_v G_v)(1+C_p N_p G_p)} \tag{3.28}$$

Let G_{vo} is open loop gain of VCM, and G_{po} is open loop gain of PZT plant. So equation 3.28 can be rewritten as equation 3.29.

$$S(s) = \frac{1}{(1+G_{vo})(1+G_{po})} \tag{3.29}$$

Where $G_{vo} = C_v N_v G_v$ and $G_{po} = C_p N_p G_p$.

From equation 3.29, the sensitivity function is the product of the sensitivity functions of VCM and PZT. In this thesis study, the VCM controller would be designed and tuned first to ensure that the VCM actuator performs in the stable region. After that the PZT controller would be designed.

3.5 Description of the Quantitative Feedback Theory (QFT)

The control design is necessary to accomplish performance specification with the presence of uncertainties such as plant changes or external disturbance. The QFT is the one of technique to design a simple low order controller with minimum bandwidth. In order to avoid problem from noise amplification, resonance and un-modeled high frequency dynamics, the specific characteristics of QFT are described

- The amount of feedback is tuned to suit for amount of plant, disturbance uncertainty and performance specifications.
- Design trade-offs at each frequency are highly transparent between stability, performance, plant uncertainty, disturbance level, controller complexity and bandwidth.
- The method extends highly intuitive classical frequency-domain loop shaping concepts to cope with simultaneous specifications and plants with uncertainties.

The quantitative feedback theory can be described with the use of a simple block diagram shown in figure 3.14. The function of each block is define as follows:

- G presents the transfer function of plant. which includes all possible variations due to uncertainties in a set $\{G\}$,
- H presents the sensor transfer function,
- C presents the controller,
- F presents the pre-filter to synthesize to meet robust stability and closed-loop specification,
- G_{dI} presents the transfer function of disturbance input,
- G_{do} presents the transfer function of disturbance output,

- d_I presents disturbance of plant input,
- d_O presents disturbance of plant output.

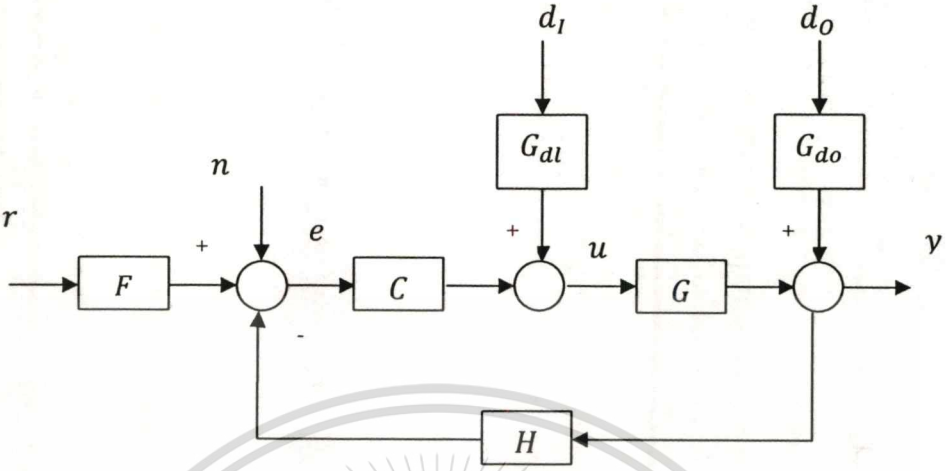

Figure 3.14 Block diagram of QFT.

The signals in the block diagram are as follow:

- n presents the sensor noise,
- r presents the reference input,
- e presents the error control input,
- u presents the control input,
- y presents the plant output respectively.

The frequency domain specifications are described in terms of transfer function as below:

1) Plant output disturbance rejection,

$$\left|\frac{y}{d_o}\right| = \left|\frac{G_{do}}{(1+CGH)}\right| < \delta_{dO} \tag{3.30}$$

Where δ_{dO} is the bounds of the disturbance output.

2) Plant input disturbance rejection,

$$\left|\frac{y}{d_I}\right| = \left|\frac{G_{dI}G}{(1+CGH)}\right| < \delta_{dI} \tag{3.31}$$

Where δ_{dI} is the bound of the disturbance input.

3) Model matching,

$$\left|\frac{y}{r-F_m}\right| = \left|\frac{CGF}{(1+CGH)} - F_m\right| < \delta_m \tag{3.32}$$

Where δ_m is the bound of the model matching.

4) Tracking,

$$\alpha \leq \left|\frac{CFG}{1+CGH}\right| \leq \beta \tag{3.33}$$

Where α and β are the upper and lower bounds of tracking.

5) Noise rejection,

$$\left|\frac{y}{n}\right| = \left|\frac{CG}{(1+CGH)}\right| < \delta_n \tag{3.34}$$

Where δ_n is the bound of the noise.

6) Control effort,

$$\left|\frac{u}{n}\right| = \left|\frac{C}{(1+CGH)}\right| < \delta_c \tag{3.35}$$

Where δ_c is the bound of the control effort.

Feedback system performance is specified in time domain, whereas the QFT is designed in frequency domain, therefore the transformation of specification from time domain to frequency domain is necessary. The frequency responses of dynamic plant G are described in the Nichols chart which is the plant template. The nominal plant is selected from center of plant template boundary. The boundary from transfer function (equation 3.30-3.35) are described the stability region which are specification criteria. In general, the nominal plant will be passing through unstable region. The Loop shaping is technique to design the controller C which is designed from open-loop transfer function to satisfy certain bounds. The design has no rule. It is up to the designer's experience. Following are basic functions that can be to use in loop shaping.

1) Simple gain: k (3.36)

2) Integrator of differentiator

$$\frac{1}{s^n} \text{ or } s^n \tag{3.37}$$

3) Lead of lag

$$\frac{\frac{s}{z}+1}{\frac{s}{p}+1} \tag{3.38}$$

4) Real pole or real zero

$$\frac{1}{\frac{s}{p}+1} \text{ or } \frac{s}{z}+1 \tag{3.38}$$

5) Complex pole or complex zero

$$\frac{1}{\frac{s^2}{\omega_n^2}+\frac{2\zeta s}{\omega_n}+1} \text{ or } \frac{s^2}{\omega_n^2}+\frac{2\zeta s}{\omega_n}+1 \tag{3.40}$$

6) Notch

$$\frac{\frac{s^2}{\omega_n^2}+\frac{2\zeta_1 s}{\omega_n}+1}{\frac{s^2}{\omega_n^2}+\frac{2\zeta_2 s}{\omega_n}+1} \tag{3.41}$$

7) Complex lead

$$\frac{s^2+2ads+a^2}{s^2+2bds+b^2}\frac{b^2}{a^2} \tag{3.42}$$

8) Super2nd

$$\frac{a_1 s^2+a_2 s+1}{b_1 s^2+b_2 s+1} \tag{3.43}$$

Design of pre-filler F is to satisfy tracking bound as shown below.

$$max_{G\epsilon\{G\}} log \left|\frac{GC(j\omega)}{1+GC(j\omega)}\right| - min_{G\epsilon\{G\}} log \left|\frac{GC(j\omega)}{1+GC(j\omega)}\right| < log \frac{\beta(\omega)}{\alpha(\omega)} \quad (3.44)$$

In other words, C reduces the variation of the closed-loop transfer function magnitude to be smaller than the specifications. F is to shift closed-loop Bode plots to be within the specification boundaries.

CHAPTER 4

Controller Design and Simulation Results

4.1 Controller design

Description of QFT was already given in the previous chapter. The detail of the design of QFT for the dual-stage actuator is explained in the chapter. There are four steps in the design of the QFT controller.

- Obtaining the plant template,
- Setting the Allowable Region and Bounds,
- Controller Loop Shaping design of the QFT controller,
- Pre-Filter Designing.

4.1.1 Obtaining the plant template

The first and important step in control design is to accurately describe for the dynamic plant. For the design of QFT, the dynamics plant is described in the frequency domain. The template is used to include the collections of uncertain plant frequency responses in various frequency injections. Figure 4.1 shows the "good" and "bad" template boundaries. There is no rule for obtaining a reasonable approximation of the boundary from the structure of the uncertain plant.

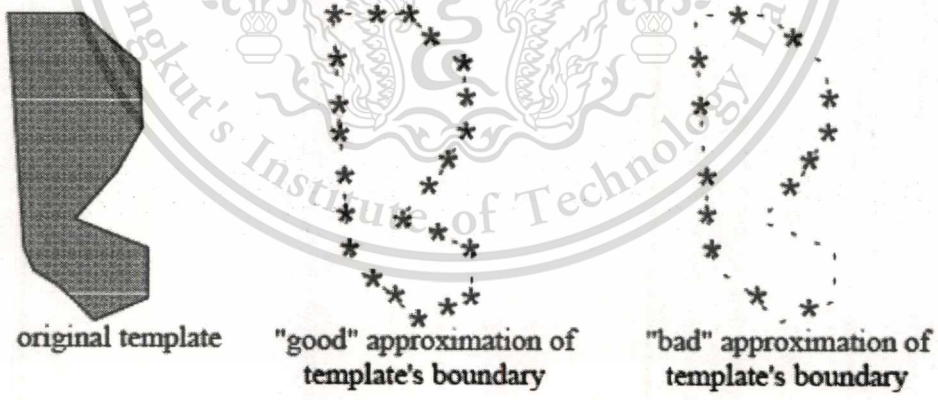

Figure 4.1 "good" and "bad" approximation of a plant template [25].

The VCM plant uncertainties are assumed to be the ±10% deviation of the value of the frequency of each resonance mode. The transfer function of all resonance modes were already given in equation 3.4-3.12. The VCM plant uncertainties could be approximated by adding the last terms of the transfer

function in equation 3.4-3.12 with $|\delta| < 10\%$. The VCM plant with uncertainties could be described by equation 4.1-4.9.

$$G_{v,1} = \frac{2.406S+1.543(1+\delta)x10^4}{S^2+49.83S+1.579(1+\delta)x10^4} \quad (4.1)$$

$$G_{v,2} = \frac{S^2+2078S+2.57(1+\delta)x10^8}{S^2+2314S+2.706(1+\delta)x10^8} \quad (4.2)$$

$$G_{v,3} = \frac{S^2+3204S+7.43(1+\delta)x10^8}{S^2+5322S+7.972(1+\delta)x10^8} \quad (4.3)$$

$$G_{v,4} = \frac{S^2+2617S+2.265(1+\delta)x10^9}{S^2+6006S+1.82(1+\delta)x10^9} \quad 4.4)$$

$$G_{v,5} = \frac{S^2+6690S+2.847(1+\delta)x10^9}{S^2+2653S+2.668(1+\delta)x10^9} \quad (4.5)$$

$$G_{v,6} = \frac{S^2+2263S+6.111(1+\delta)x10^9}{S^2+1364S+6.83(1+\delta)x10^9} \quad (4.6)$$

$$G_{v,7} = \frac{S^2-7.238x10^4S+3.683(1+\delta)x10^9}{S^2+9.338x10^4S+5.806(1+\delta)x10^8} \quad (4.7)$$

$$G_{v,8} = \frac{S^2+1.048x10^4S+1.601(1+\delta)x10^{10}}{S^2+1980x10^4S+1.498(1+\delta)x10^{10}} \quad (4.8)$$

$$G_{v,9} = \frac{S^2+2.341x10^4S+1.809(1+\delta)x10^{10}}{S^2+3935S+1.974x(1+\delta)10^{10}} \quad (4.9)$$

The sweep sine inputs are injected to the VCM plant with uncertainties. The responses are plot into the Nichols chart as shown in figure 4.2. The response boundary of each mode of sweep sine input will indentify the area of plant with uncertainties. In this thesis study, only one plant which is inside the center the plant template boundary is used, and is called as the nominal plant. The nominal plant is shown as the solid line plot in figure 4.2.

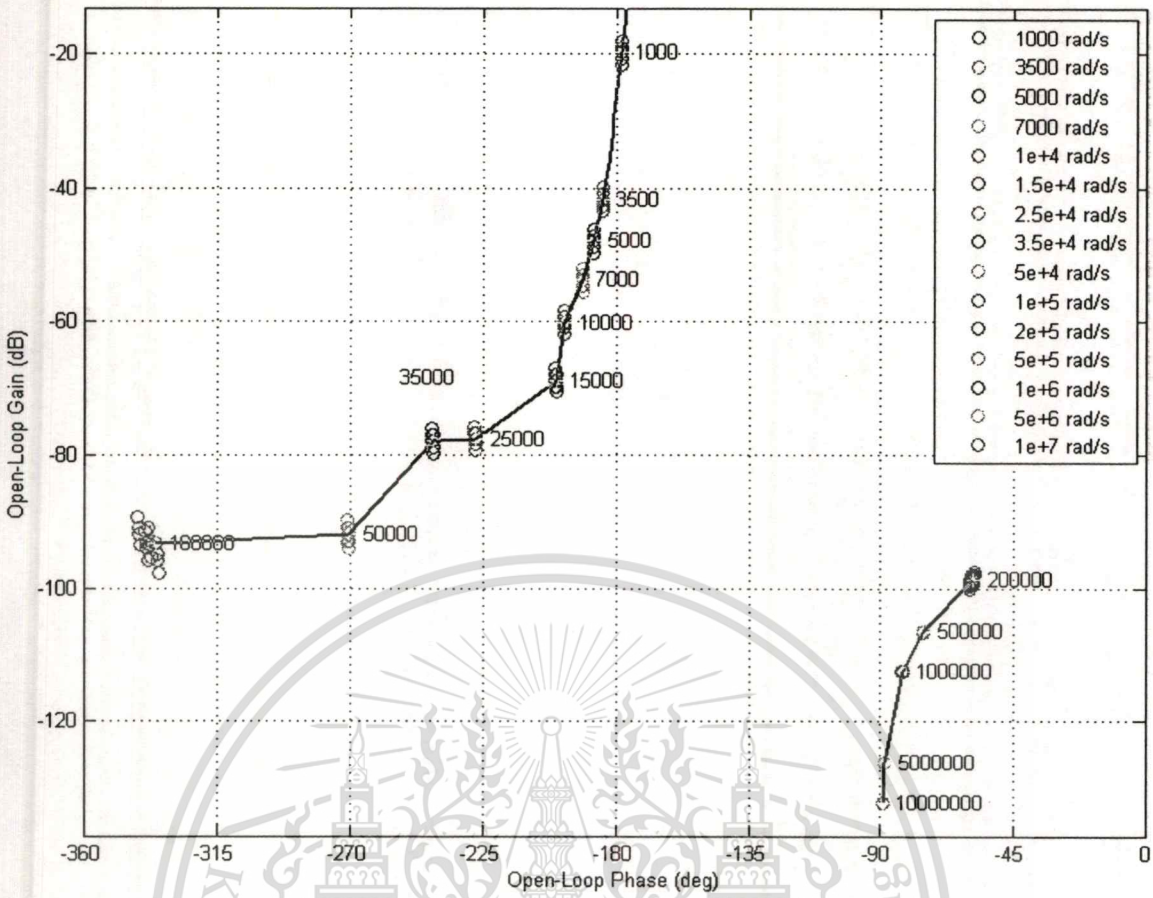

Figure 4.2 Plant template of the VCM.

In The same fashion, the PZT plant uncertainties are approximated by adding $|\delta| < 10\%$ to the last terms of equation 3.14-3.18 to obtain equation 4.10-4.14.

$$G_{p,1} = \frac{-1.696x10^{-9}S+1.039(1+\delta)}{S^2+2.163x10^4S+2.336(1+\delta)x10^9} \tag{4.10}$$

$$G_{p,2} = \frac{S^2+3896S+2.945(1+\delta)x10^9}{S+4.459(1+\delta)x10^4} \tag{4.11}$$

$$G_{p,3} = \frac{S^2-1423S+7.041(1+\delta)x10^9}{S^2+9783S+6.734(1+\delta)x10^9} \tag{4.12}$$

$$G_{p,4} = \frac{S^2-1.998x10^4S+1.2(1+\delta)x10^{10}}{S^2+1.671x10^4S+1.14(1+\delta)x10^{10}} \tag{4.13}$$

$$G_{p,5} = \frac{S^2+4045S+2.096(1+\delta)x10^{10}}{S^2+4065S+2.096(1+\delta)x10^{10}} \tag{4.14}$$

Figure 4.3 shows the PZT plant template by various the sweep sine frequencies and its nominal plant template (solid line).

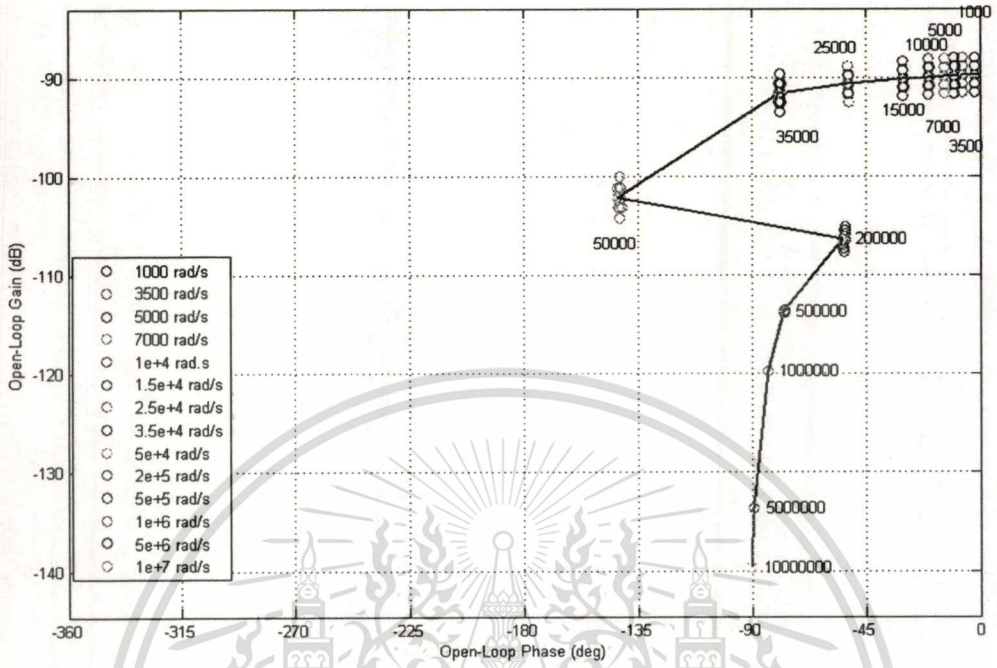

Figure 4.3 Plant template of the PZT.

4.1.2 Settling the Allowable Region and Bounds

Three common types of bounds are shown in both complex plan and Nichols chart in figure 4.4. The input sweep sine ω_i would be injected to the $C(j\omega)G(j\omega)$ which is the open loop system transfer function. The shaded region is unallowed zone, and the controller must be shaped out of the shaded region.

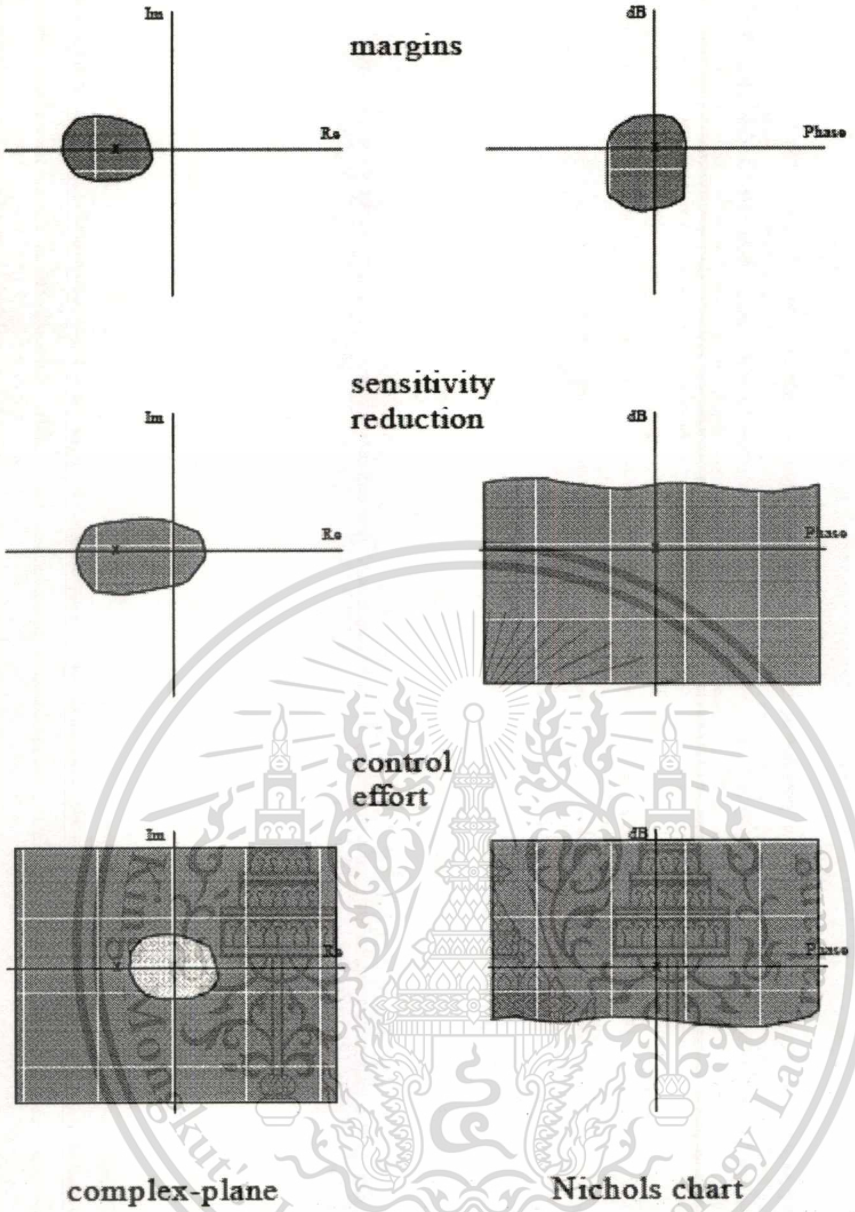

Figure 4.4 Common type of QFT bound on complex plane and Nichols chart.

The control performances needed from the QFT in this thesis study are disturbance rejection and tracking performances, whose bounds are described by equation 3.30 and 3.33 respectively. Renaming the output Y with PES and setting G_{dI}=1 , G_{do}=1, and P_{ref}=0 (figure 3.12,3.13) the equation 3.30 can be rewritten as equation 4.25 to define the disturbance rejection bound.

$$\frac{PES}{r} = \left|\frac{1}{1+CG}\right| \tag{4.25}$$

δ for the disturbance rejection is set to be 10 dB according to the stability margin specification.

$$\left|\frac{1}{1+CG}\right| < \delta \, , \delta \geq 10 \tag{4.26}$$

The bounds for sensitivity of VCM and PZT are then obtained and plot in the Nichols chart as show in figure 4.5 and 4.6. Sweep sine inputs are injected in the equation 4.26 with G_v of VCM and G_p of PZT.

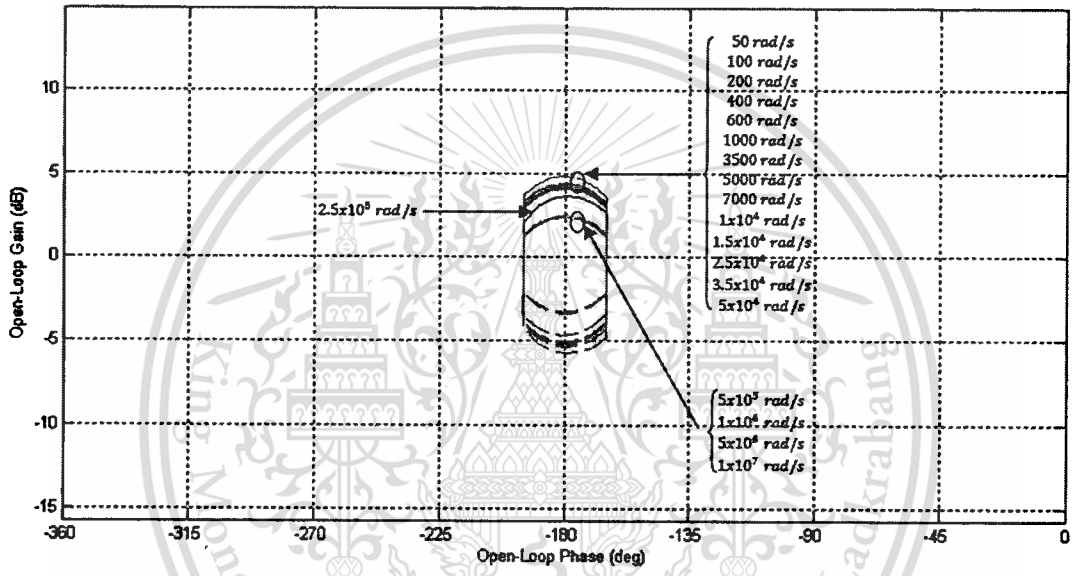

Figure 4.5 VCM bounds of boundary of sensitivity.

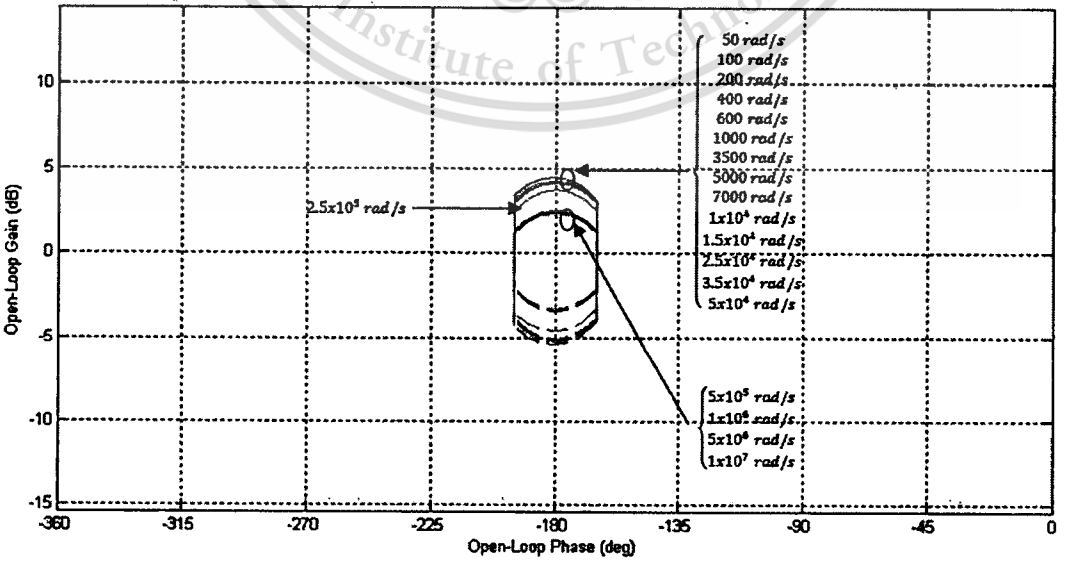

Figure 4.6 PZT bounds of boundary of sensitivity.

The bounds for tracking of VCM and PZT are then obtained and plot in the Nichols chart as show in figure 4.7 and 4.8. Sweep sine inputs are injected in the equation 4.27 with G_v of VCM and G_p of PZT. The tracking bounds are represented below.

$$\alpha \leq \left|\frac{CFG}{1+CG}\right| \leq \beta \tag{4.27}$$

Where G is represented the nominal plant,

- F presents the pre-filter which setting to 1,
- c presents the controller which setting to 1,
- α presents the upper tracking boundary from equation $\frac{\omega_n^2}{S+2\xi\omega_n S+\omega_n^2}$; which assumes upper tacking bandwidth is 10000 rad/s and damping ratio is 1($\{\omega_n, \xi\} = \{1x10^4, 1\}$),
- β presents the lower tracking boundary from equation $\frac{\omega_n^2}{S+2\xi\omega_n S+\omega_n^2}$, which assumes lower tracking bandwidth is 10000 rad/s and damping ratio is 0.7($\{\omega_n, \xi\} = \{1x10^4, 0.7\}$).

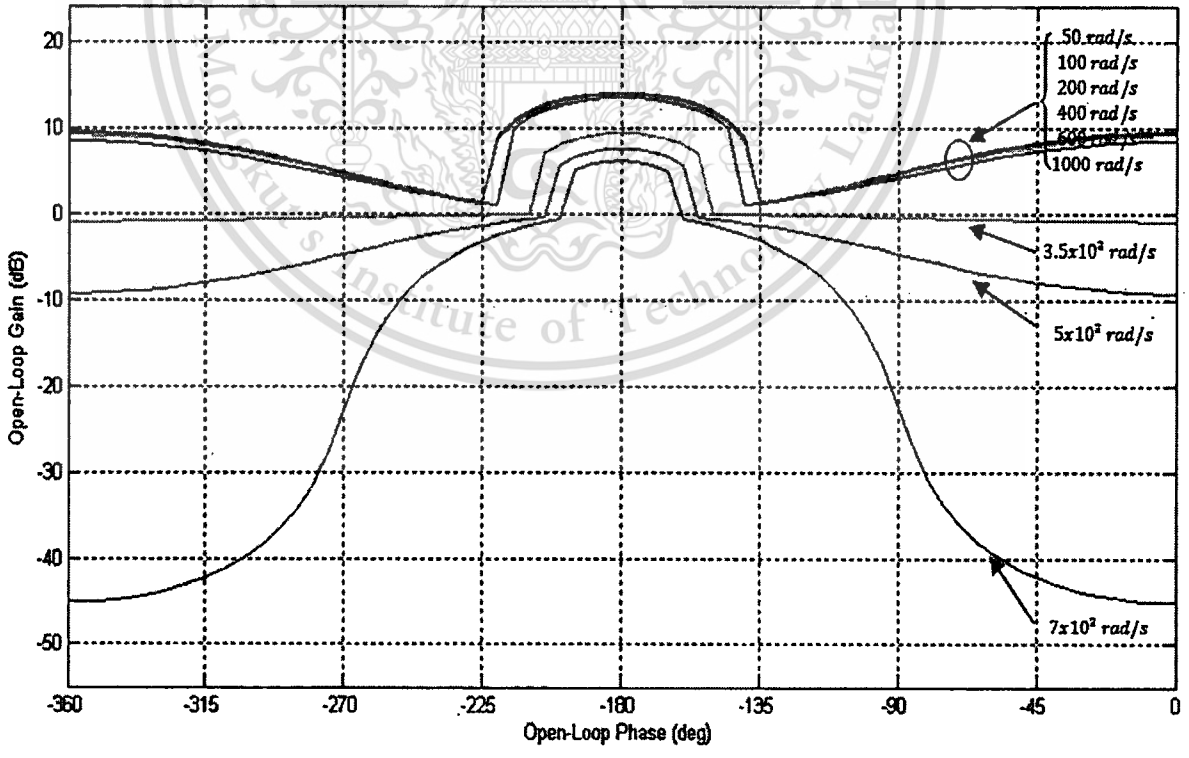

Figure 4.7 VCM bounds of tracking boundary.

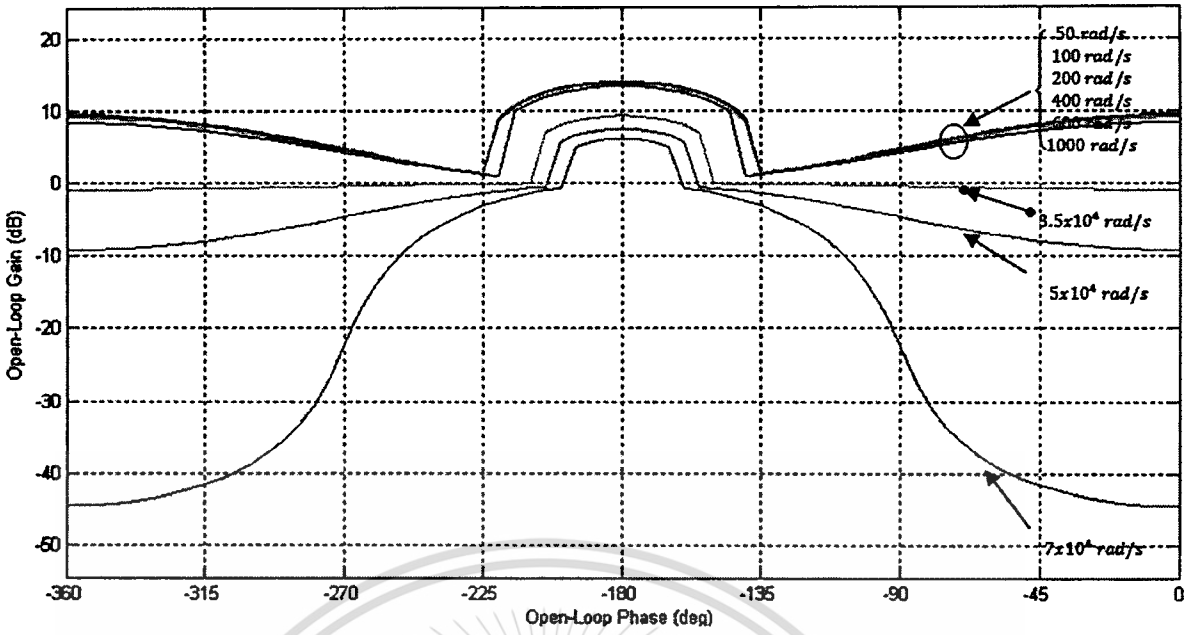

Figure 4.8 PZT bounds of tracking boundary.

The intersections of the two boundaries of disturbance and tracking bounds create the strictest bound, which is used for open-loop shaping to satisfy at various designed frequencies. The picture 4.9 and picture 4.10 are show the VCM and PZT bounds of worst case intersection between the tracking boundary and the sensitivity boundary.

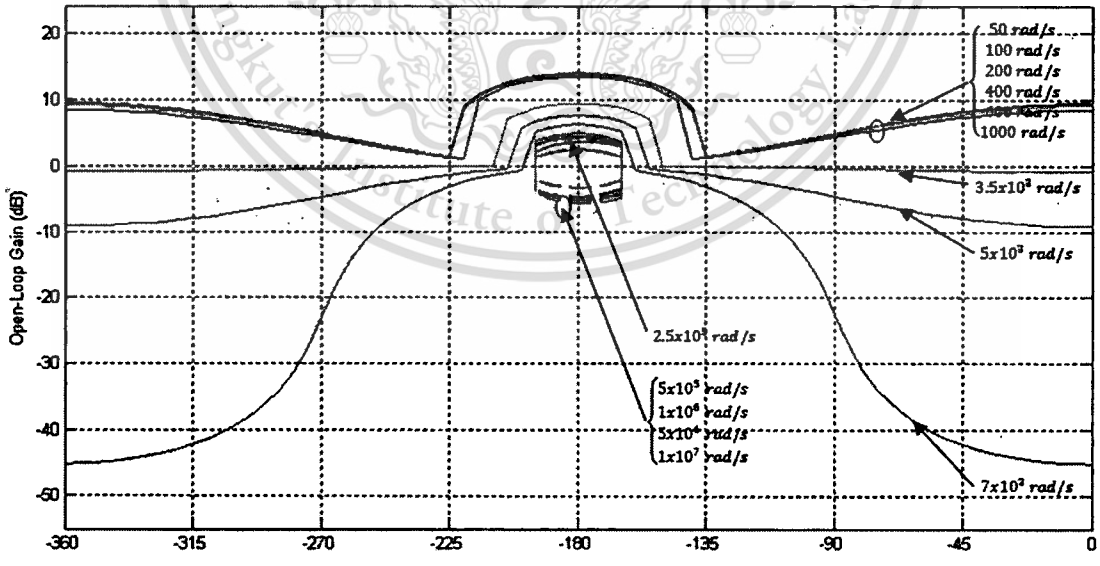

Figure 4.9 VCM bounds of worst case intersection between tracking and sensitive boundary.

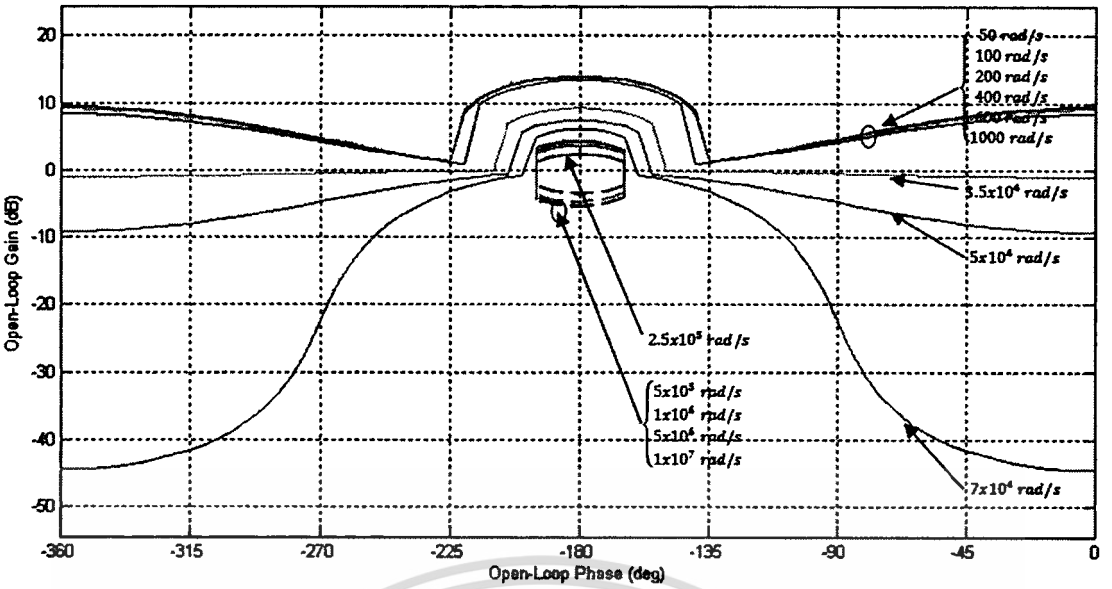

Figure 4.10 PZT bounds of worst case intersection between tracking and sensitive boundary.

4.1.3 Loop Shaping

The open loop shaping is CG where C=1. The strictest bounds at various frequency shown in figure 4.11(a) is of the VCM before loop shaping. The nominal plant is shown in dotted line. It passes through unstable region that meaning the system is unstable (figure 4.11(a)). Therefore the controller C is needed to stabilize the system. The VCM controller, $c_v(s)$, is shaped to servo loop by trial and error and consists of the following functions.

- Gain k is equal $5.586x10^5$ (equation 3.36),
- Integrator $\frac{1}{s}$ (equation 3.37),
- Real zero is $\left(\frac{s}{5.228x10^4}+1\right),\left(\frac{s}{3727}+1\right),\left(\frac{s}{2360}+1\right)$ (equation 3.39),
- Complex zero is $\left(\frac{s^2}{1.547x10^5}+\frac{0.4384s}{1.547x10^5}+1\right)$ (equation 3.40),
- Complex pole is $\frac{1}{\left(\frac{s^2}{1.612x10^5}+\frac{0.74396s}{1.612x10^5}+1\right)\left(\frac{s^2}{4.028x10^4}+\frac{0.703s}{4.028x10^4}+1\right)}$ (equation 3.40).

The controller of VCM, $c_v(s)$ is the product of all the previous functions.

$$c_v(s) = \frac{5.586x10^5\left(\frac{s}{5.228x10^4}+1\right)\left(\frac{s}{3727}+1\right)\left(\frac{s}{2360}+1\right)\left(\frac{s^2}{1.547x10^5}+\frac{0.4384s}{1.547x10^5}+1\right)}{s\left(\frac{s^2}{1.612x10^5}+\frac{0.74396s}{1.612x10^5}+1\right)\left(\frac{s^2}{4.028x10^4}+\frac{0.703s}{4.028x10^4}+1\right)}$$

$$= \frac{2138s^5 + 4.149x10^8s^4 + 6.882x10^{13}s^3 + 3.084x10^{18}s^2 + 1.688x10^{22}s + 2.354x10^{25}}{s^5 + 1.983x10^5s^4 + 3.563x10^{10}s^3 + 1.7x10^{15}s^2 + 4.21x10^{19}s} \quad (4.28)$$

The result after adding controller C_v is shown on figure 4.11(b). The response of each mode of sweep sine input is in the stable area. Therefore, the VCM plant with controller C_v would be stable for the operation of all frequency ranges.

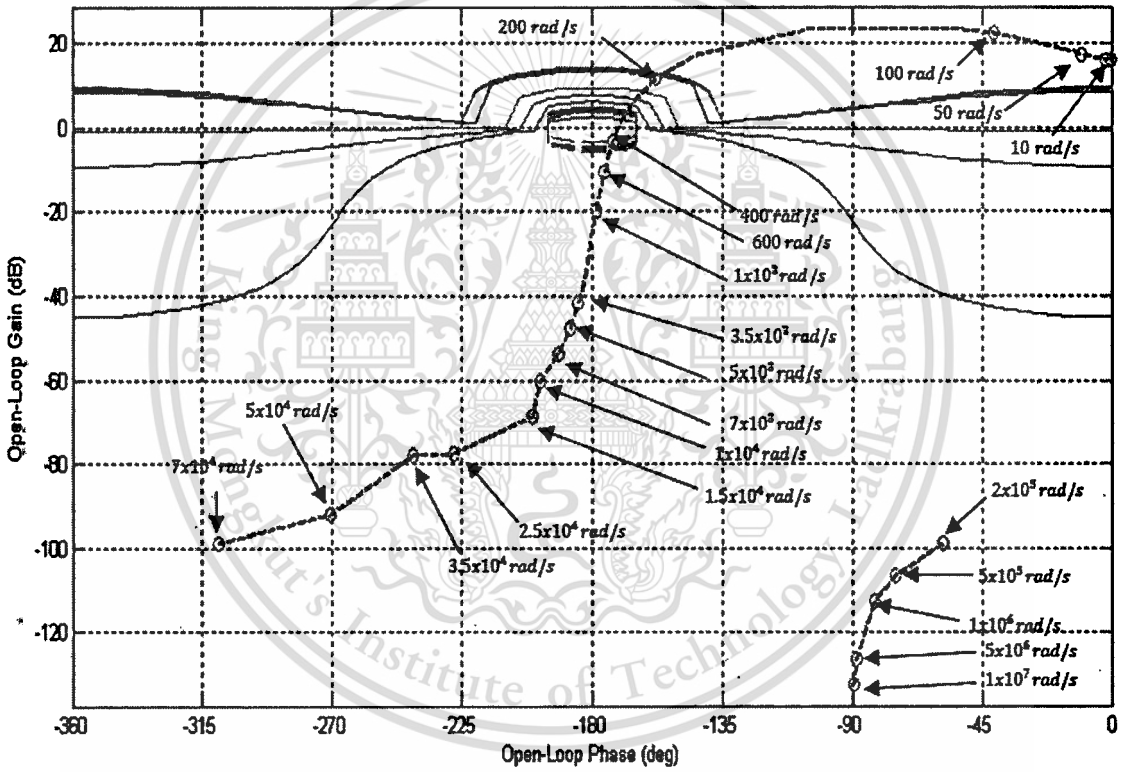

(a)

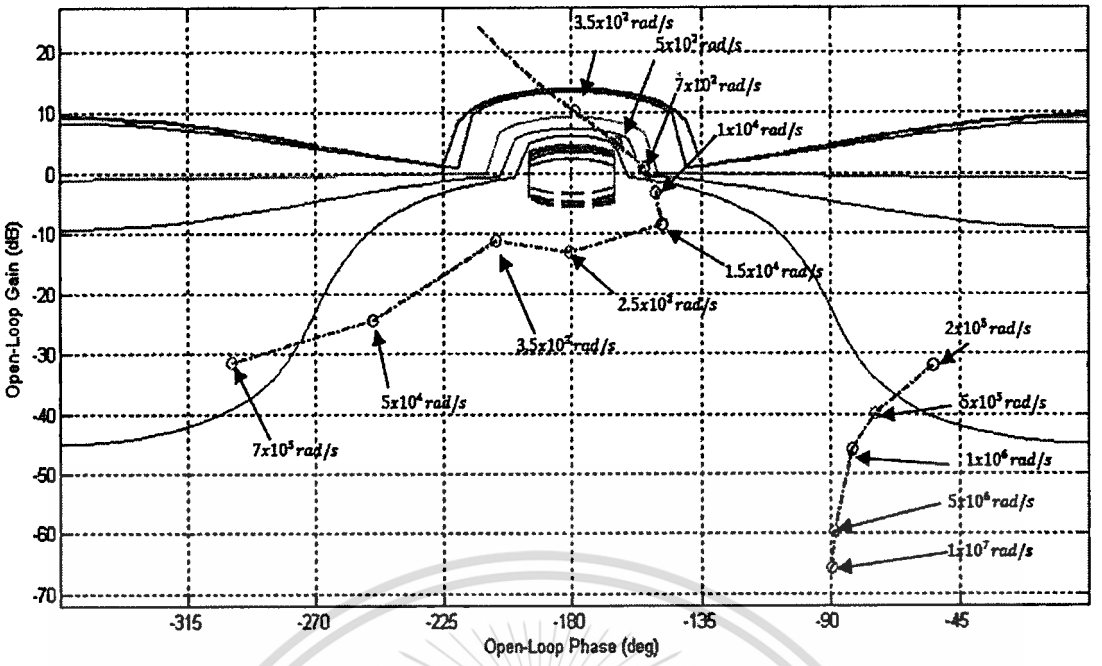

(b)

Figure 4.11 VCM loop shaping, (a) before loop shaping, (b) after loop shaping.

For PZT controller, The controller is shaped to servo loop by trial and error and consists of the following functions.

- Gain k is equal $1.935x10^5$ (equation 3.36)
- Real zero is $\left(\frac{s}{2.636x10^5}+1\right), \left(\frac{s}{3.055x10^4}+1\right)$ (equation 3.39)
- Real pole is $\frac{1}{\left(\frac{s}{2.636x10^5}+1\right)\left(\frac{s}{2960}+1\right)}$ (equation 3.39)
- Complex zero is $\left(\frac{s^2}{1.53x10^5}+\frac{0.417s}{1.53x10^5}+1\right)$ (equation 3.40)
- Complex pole is $\left(\frac{s^2}{1.599x10^5}+\frac{0.424s}{1.599x10^5}+1\right)$ (equation 3.40)

The controller of PZT, $c_p(s)$ is the product of all the previous functions.

$$c_p(s)=\frac{1.935x10^5\left(\frac{s}{2.636x10^5}+1\right)\left(\frac{s}{3.055x10^4}+1\right)\left(\frac{s^2}{1.53x10^5}+\frac{0.417s}{1.53x10^5}+1\right)}{\left(\frac{s}{2.636x10^5}+1\right)\left(\frac{s}{2960}+1\right)\left(\frac{s^2}{1.599x10^5}+\frac{0.424s}{1.599x10^5}+1\right)}$$

$$= \frac{2.046x10^4s^4 + 8.635x10^9s^3 + 1.413x10^{15}s^2 + 1.619x10^{22}s + 3.857x10^{24}}{s^4 + 4.021x10^5s^3 + 6.247x10^{10}s^2 + 6.916x10^{15}s + 1.993x10^{19}} \quad (4.29)$$

The result of before and after loop shaping of PZT actuator are shown in figure 4.11 (a) and figure 4.11(b) respectively.

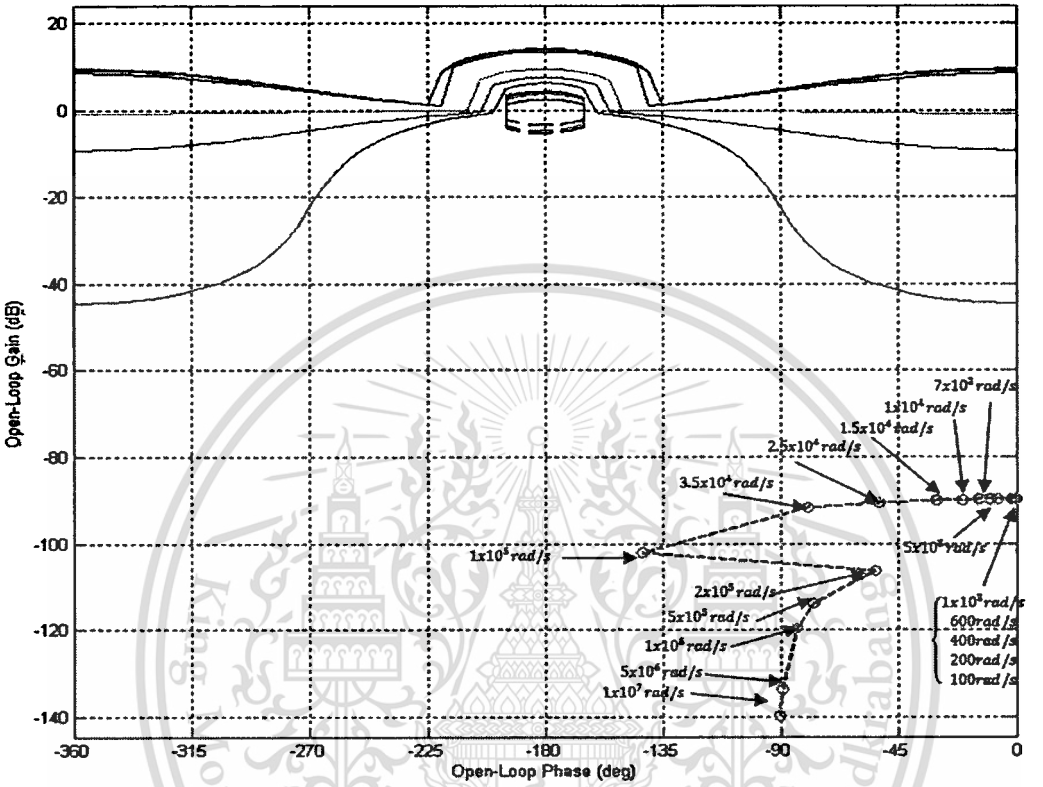

(a)

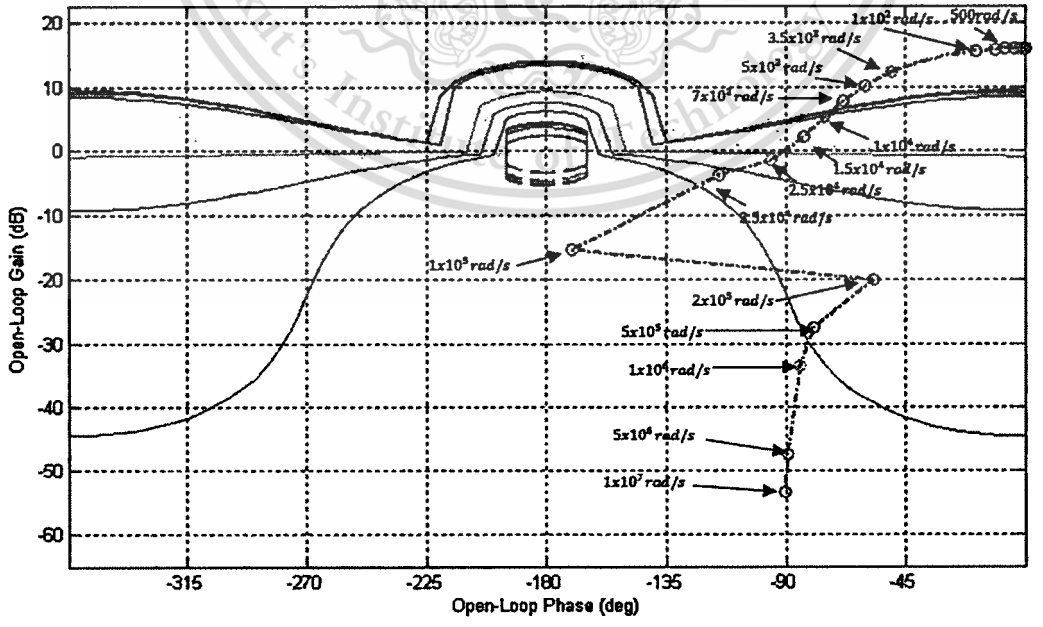

(b)

Figure 4.12 PZT loop shaping, (a) before loop shaping, (b) after loop shaping.

4.1.4 Pre-Filter

The solid line in figure 4.13 is the frequency response of the closed loop system with integrated controllers c_v and c_p. The performance of the closed loop system is still out α and β tracking bounds which are shown as dashed line (figure 4.13). In order that the tracking of the control system would perform in the α - β bounds, a pre-filter is added to the closed loop system.

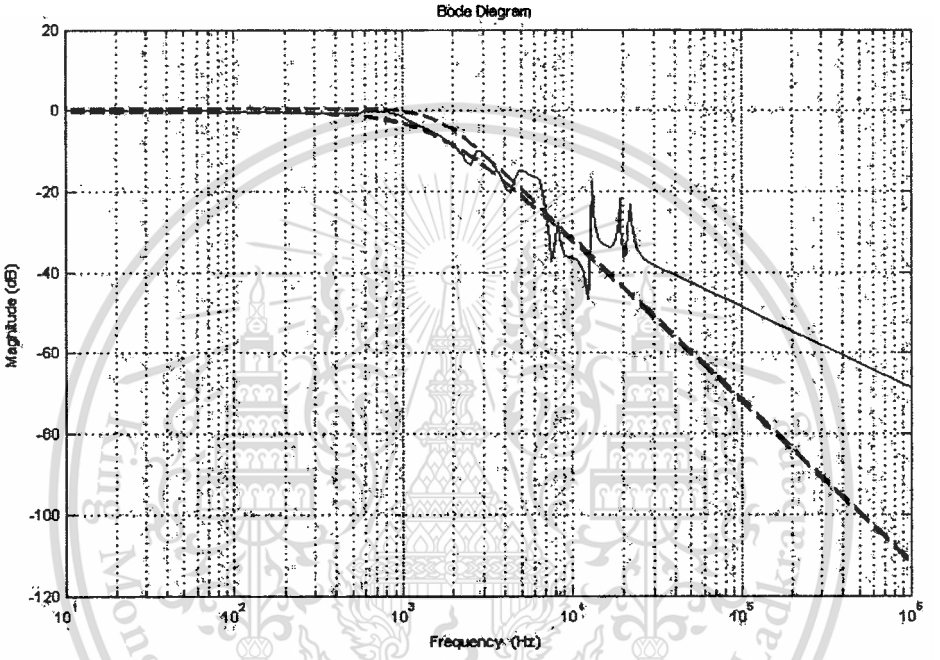

Figure 4.13 Close loop shape before appending the pre-filter

By trial and error, the pre-filter could be obtained as

$$F(s) = \frac{0.4577s^3+4755s^2+3.38x10^7s+1.493x10^{11}}{s^3+10047s^2+7.033x10^7s+1.493x10^{11}} \quad (4.30)$$

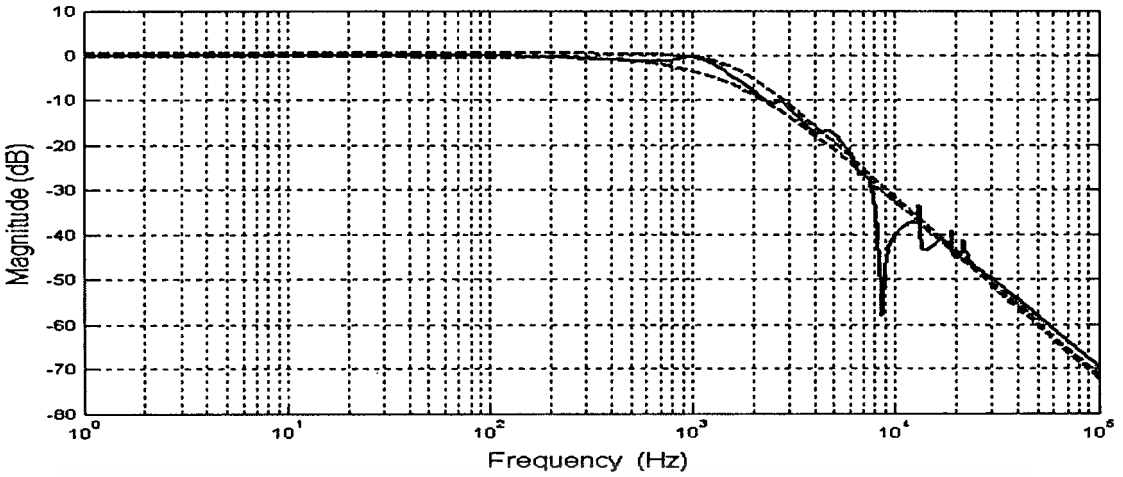

Figure 4.14 Close loop shape after appending the pre-filter

After pre-filler is added, the tracking performance of the control system is within the tracking bounds as can be seen in figure 4.14. The solid line which is the frequency response of the control system stays well within the tracking bounds (dashed line).

4.2 Computer simulations

The performance criteria requirements of the proposed dual-stage actuator control system are listed below:

- The overshoot of the actual displacement must be less than 5%.
- The mean of the steady-state error must be zero.
- The gain and phase margins must be greater than 6dB and 30°.
- The maximum peaks of the sensitivity must be less than 10dB.
- The settling time of the step response must be as short as possible.

The step responses of dual-stage actuator with PID and QFT are shown in figure4.5. The step response of the QFT control system is shown in the solid line, whereas one of the PID control system is shown in the dotted line. The overshoot of the QFT controller is 0.7% better than that of 9.8% of PID control system. This means that the read/write head seeking time of QFT control system is faster than the PID control system.

The steady state error of both control system are zeros. However the setting time (at ± 5% of steady state value) of the QFT control is 0.934 ms which is much faster than that of 2.09 ms of the PID control. This means that the read/write head command of the QFT control system could then be much faster declared than the PID control system.

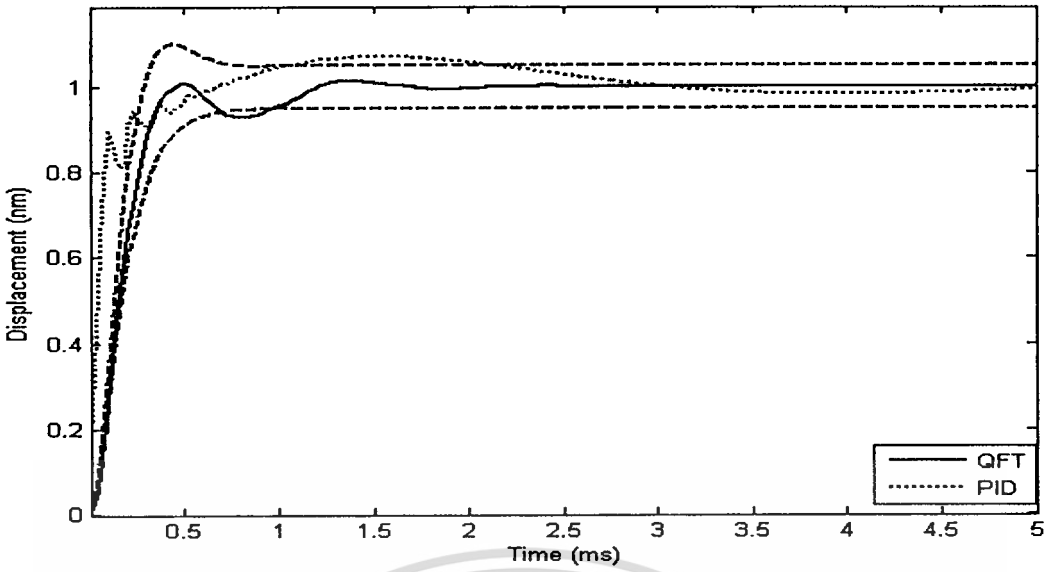

Figure 4.15 The step responses comparison between PID and QFT technique.

The frequency responses of the open loop transfer function of QFT control system is shown in figure 4.16. The gain and phase margins can be measured from the plot to be 8.7 dB and 57°, respectively. Both values are within the performance criteria requirement.

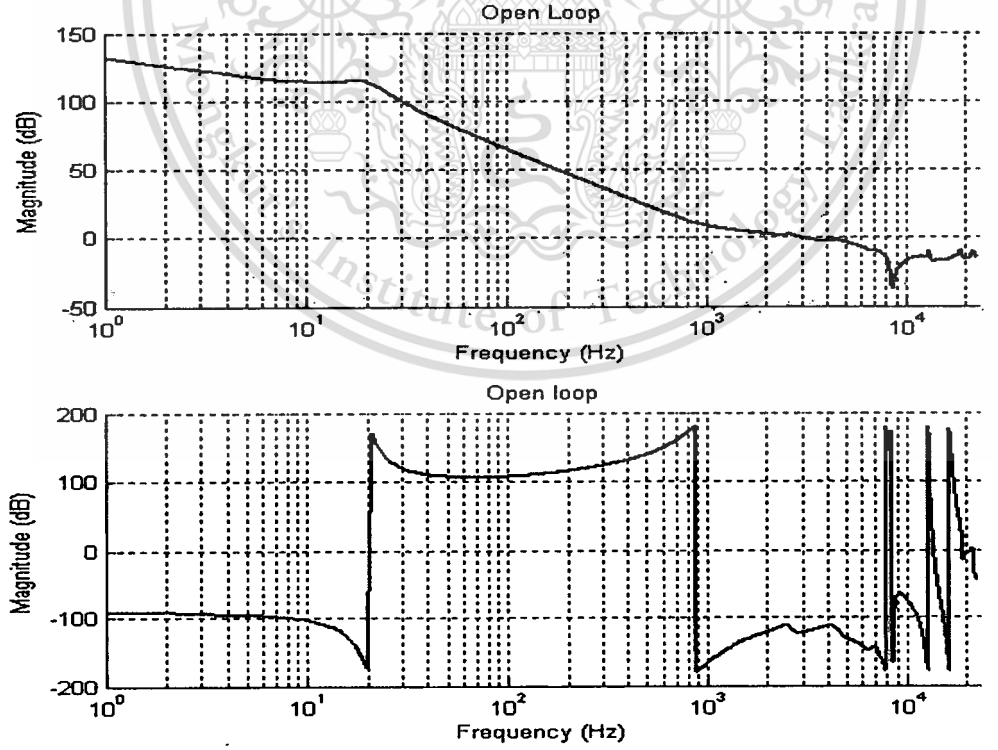

Figure 4.16 The open-loop BODE plot of the QFT control system.

Figure 4.17 shows the sensitivity function of dual-stage actuator are less than 10 dB.

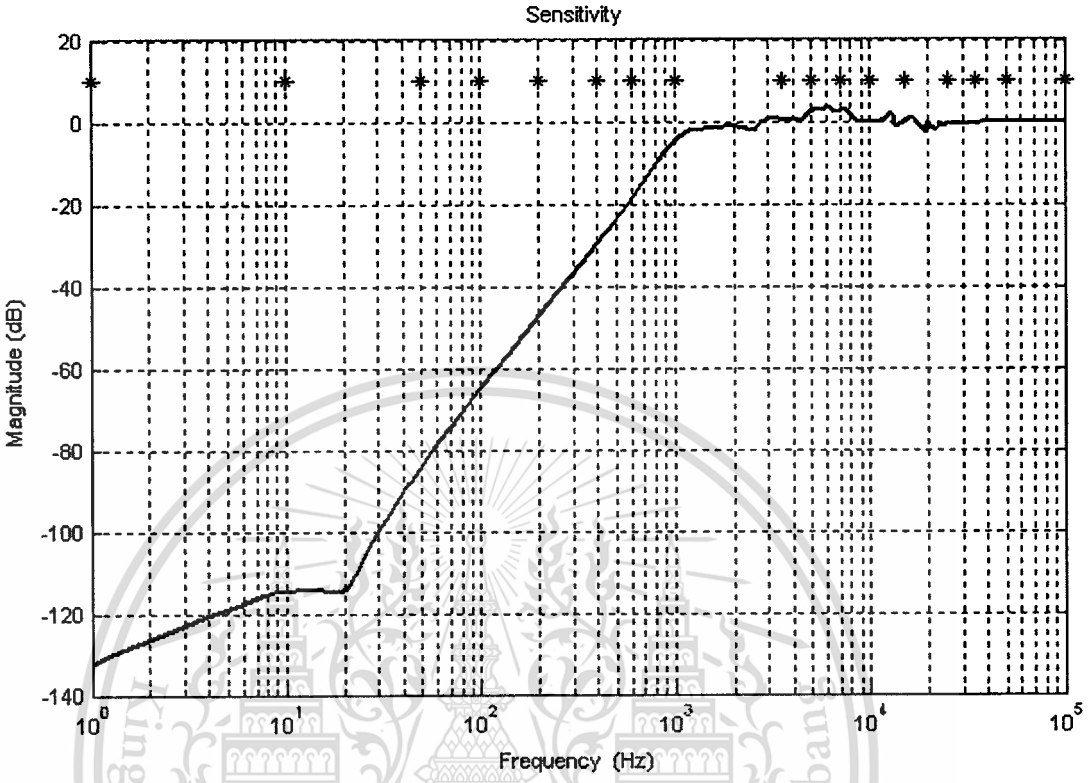

Figure 4.17 The result of sensitivity function

Figure 4.18 shows the RRO disturbance rejections of PID and QFT technique. The RRO disturbance rejection of the QFT is approximately thirty times better than PID technique. The ability of rejecting the disturbances such as mechanical component vibrations or electrical noises could decrease the size of track pitch. Therefore the QFT controller is proved to be a potential control technique for developing a higher areal density HDD.

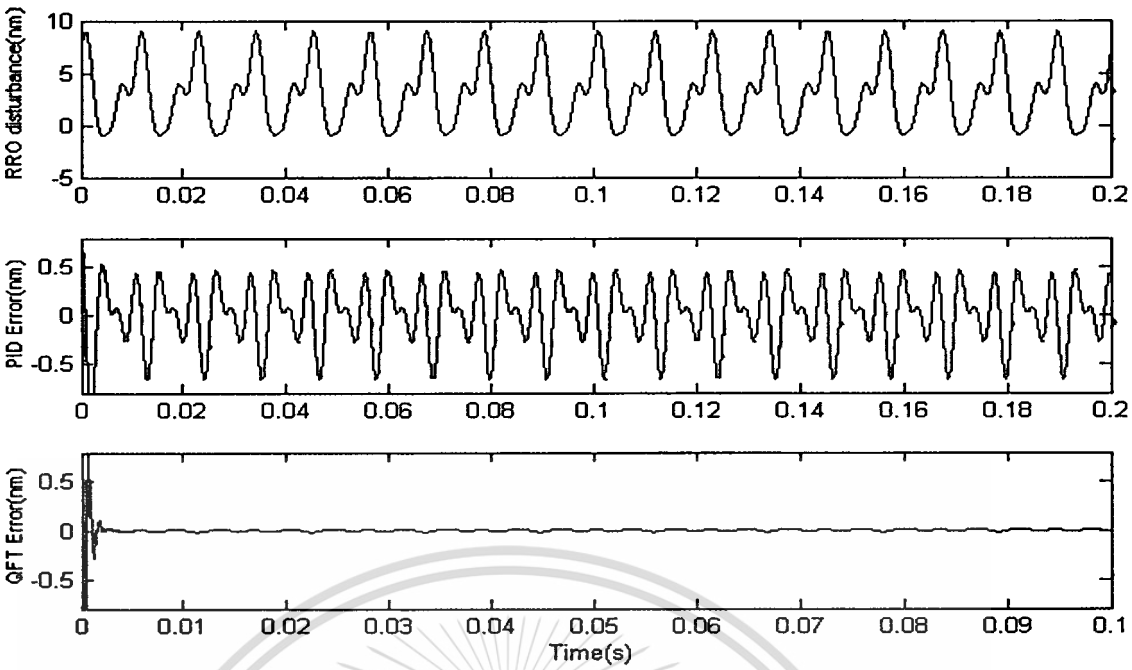

Figure 4.18 The RRO disturbance rejection comparison between PID and QFT techniques.

CHAPTER 5
Conclusion

5.1 Conclusion

The system identification of dual-stage actuator was obtained on frequency domain. The model of the VCM actuator is of 18 orders, where of the model of the PZT actuator is of 10 orders. The models were verified by comparing the actual PES signals to the computed ones. The frequencies and magnitudes of both data were well agreed.

The controller designs based on decoupling and QFT control were successfully implemented. The performances achieved are listed below.

- The over shoot was 0.7%.
- The steady state error is zero.
- The gain and phase margins are 8.7 dB and 57° respectively.
- The settling time 0.934 ms.

The settling time of the QFT control system is 0.934 ms faster than that of the PID control system. The disturbances rejection of the QFT control system is 30 times better than that of the PID control system. These mean that the track width could be much smaller with the implementation of the QFT control.

REFERENCES

[1] Al Mamun, T. H. Lee, and T. S. Low, "Frequency domain identification of transfer function model of a disk drive actuator," Mechatronics, vol. 12, pp. 563-574, May 2002.

[2] G. Y. Cheng, K. M. Peng, B. M. Chen, and T. H. Lee, "A microdrive track following controller design using robust and perfect tracking control with nonlinear compensation," Mechatronics, vol. 15, pp. 933-948, Oct 2005.

[3] H. Numasato and M. Tomizuka, "Settling control and performance of a dual-actuator system for hard disk drives," Ieee-Asme Transactions on Mechatronics, vol. 8, pp. 431-438, Dec 2003.

[4] K. Peng, B. M. Chen, T. H. Lee, and V. Venkataramanan, "Design and implementation of a dual-stage actuated HDD servo system via composite nonlinear control approach," Mechatronics, vol. 14, pp. 965-988, Nov 2004.

[5] K. C. Tan, R. Sathikannan, W. W. Tan, and A. P. Loh, "Evolutionary design and implementation of a hard disk drive servo control system," Soft Computing, vol. 11, pp. 131-139, Jan 2007.

[6] M. Vagia, G. Nikolakopoulos, and A. Tzes, "Design of a robust PID-control switching scheme for an electrostatic micro-actuator," Control Engineering Practice, vol. 16, pp. 1321-1328, Nov 2008.

[7] Yamaguchi, T.; "HDD servo control development - Present and future" SICE-ICASE, 2006. International Joint Conference Publication Year: 2006 , Page(s): 2756 - 2759 [1-6]

[8] Shangying Zhang; Xuedong Chen; Haihua Mu; Hui Zhao; "Quantitative feedback control of a linear positioning stage with cogging force compensation" Nano/Micro Engineered and Molecular Systems, 2008. NEMS 2008. 3rd IEEE International Conference on Publication Year: 2008 , Page(s): 660 – 663

[9] Du, C., L. Xie, J. Zhang, and G. Guo. 2008. Disturbance Rejection for a Data Storage System via Sensitivity Loop Shaping and Adaptive Nonlinear Compensation. IEEE/ASME Transactions on Mechatronics. Vol. 13. No. 5. pp. 493-501.

[10]Horowitz, I. 1959. Fundamental Theory of Linear Feedback Control Systems. Trans IRE on Auto Control. AC-4.

[11]Levin, J. and P. Ioannou. 2009. Adaptive Mode-Suppression and Disturbance-Rejection Scheme with Application to Disk Drives. IEEE Transactions on Control Systems Technology. Vol. 17. No. 3. pp. 620-632.

[12]Low, K.S. and T.S. Wong. 2007. A Multiobjective Genetic Algorithm for Optimizing the Performance of Hard Disk Drive Motion Control System. IEEE Transactions on Industrial Electronics. Vol. 54. No. 3. pp. 1716-1725.

[13]Ohno, K. and T. Hara. 2006. Adaptive Resonant Mode Compensation for Hard Disk Drives. IEEE Transactions on Industrial Electronics. Vol. 53. No. 2. pp. 624-630.

[14]Park, S.W., J. Jeong, H.S. Yang, Y.P. Park, and N.C. Park. 2005. Repetitive Controller Design for Minimum Track Misregistration in Hard Disk Drives. IEEE Transactions on Magnetics. Vol. 41. No. 9. pp. 2522-2528.

[15]Taghirad, H.D. and E. Jamei. 2008. Robust Performance Verification of Adaptive Robust Controller for Hard Disk Drives. IEEE Transactions on Industrial Electronics. Vol. 55. No. 1. pp. 448-456.

[16]Yao, B. 1997. High Performance Adaptive Robust Control of Nonlinear Systems: A General Framework and New Schemes. Proc IEEE Conf Decision Control. San Diego. CA. pp. 2489-2494.

[17]You, K.H. and M. Hong. 2007. Robust Linear Quadratic Sliding-Mode Control for Hard Disk Drives. IEEE Transactions on Instrumentation and Measurement. Vol. 56. No. 3. pp. 1087-1093.

[18]Zheng, Q. and M. Tomizuka. 2007. Compensation of Dominant Frequency Components of Nonrepeatable Disturbance in Hard Disk Drives. IEEE Transactions on Magnetics. Vol. 43. No. 9. pp. 3756-3762.

[19] Kyoung Kwan Ahn, Nguyen Huynh Thai Chau. 2007. Design of a robust force controller for the new mini motion package using quantitative feedback theory. Science Direct on Mechatronics 17(2007) 542-550.

[20]Masaki Nagashima and Shinsuke Nakagawa. 2008. I Identification of Microactuator Resonance at Frequencies Beyond the Nyquist Rate in Dual-Stage Actuator Hard Disk Drives. SICE Annual Conf 2008, Japan, Aug20-22, 2008

[21]Roberto Horowitz et al., Dual-stage servo systems and vibration compensation in computer hard disk drives, Control Engineering Practice (2006), doi:10.1016/j.conengprac.2006.09.003

[22]Ben M. Chen, Tong H. Lee, Kemao Peng, and V. Venkataramanan, *Hard Disk Drive Servo Systems 2nd Edition*, October 2005

[23]Oded Yaniv, Quantitative *Feedback Design of Linear and Nonlinear Control System 1st Edition*, Kluwer Academic Publishers, 1999

[24]Mamun, Guo G.,Bi C., *Hard Disk Drives Mechatronics and Control*, CRC press, 2007

[25] Borghesani C, Chait Y, and Yaniv O, *The QFT Frequency Domain Control Design Toolbok, 3rd Edition*, July 2003

APPENDIX
INTERNATIONAL CONFERENCE

P-6

Track Following Control of HDD Dual Stage Actuator Using Quantitative Feedback Theory

T. Aryurawattana[1], W. Chatlatanagulchai[2], and U. Pinsopon[3]
[1]College of Data Storage Technology and Applications
[1,3]King Mongkut's Institute of Technology, Bangkok 10520, Thailand
E-mail: S2600619@kmitl.ac.th
[2]Data Storage Technology Research Unit
Kasetsart University, Bangkok 10900, Thailand
E-mail: fengwtc@ku.ac.th
[3]Faculty of Engineering and College of Data Storage Technology and Applications
E-mail: kpunnat@kmitl.ac.th

Abstract— The trend of hard disk drive (HDD) requires increasing areal density that resulting in bit size and the track pitch at media must be smaller. The controller design for track-seeking and track-following has to achieve target in the control of the servo mechanism. This paper is about track-following control of the read/write head and allowing them to stay in the middle of the track. The boundary of position can be read or write within +10% of track in the presence of external disturbance. The control design for track following must pass increased ability to reject disturbance, which is the one method to increase a hard disk drive's capacity. In this paper we present quantitative feedback theory, a technique for track following control. The plant for design prefer dual state actuator and the control design has base on frequency domain. The design was completed using Matlab tools for design and simulation. The proposed control technique is able to reduce 50% of settling time and is thirty times more capable in attenuating repeatable runout disturbance.

Keywords— Hard Disk Drive, Track Following, Quantitative Feedback Theory, Disturbance Rejection.

Track Following Control of HDD Dual Stage Actuator Using Quantitative Feedback Theory

T. Aryurawattana [1], W. Chatlatanagulchai[2], and U. Pinsopon[3]
[1]College of Data Storage Technology and Applications
[1,3]King Mongkut's Institute of Technology, Bangkok 10520, Thailand
e-mail: S2600619@kmitl.ac.th
[2]Data Storage Technology Research Unit
Kasetsart University, Bangkok 10900, Thailand
e-mail: fengwtc@ku.ac.th
[3]Faculty of Engineering and College of Data Storage Technology and Applications
e-mail: kpunnat@kmitl.ac.th

Abstract—**The trend of hard disk drive (HDD) requires increasing areal density that resulting in bit size and the track pitch at media must be smaller. The controller design for track-seeking and track-following has to achieve target in the control of the servo mechanism. This paper is about track-following control of the read/write head and allowing them to stay in the middle of the track. The boundary of position can be read or write within ±10% of track in the presence of external disturbance. The control design for track following must pass increased ability to reject disturbance, which is the one method to increase a hard disk drive's capacity. In this paper we present quantitative feedback theory, a technique for track following control. The plant for design prefer dual state actuator and the control design has base on frequency domain. The design was completed using Matlab tools for design and simulation. The proposed control technique is able to reduce 50% of settling time and is thirty times more capable in attenuating repeatable runout disturbance.**

*Keywords-component; —**Hard Disk Drive, Track Following, Quantitative Feedback Theory, Disturbance Rejection.***

I. INTRODUCTION

To achieve a high recording density, the control technology has to be improved to enable the read/write head to stay in middle of the track (on track condition). The track following performance is a major factor in increasing the hard disk drive's capacity on high recoding density. In order to perform read/write head operation, the read/write head must be positioned within the steady state error boundary at all times in the presence of external disturbance and the plant with uncertainty. The control technique must be robust for disturbance rejection and uncertainty. There are two external disturbance that affect system, namely repeatable run out (RRO) and non-repeatable run out (NRRO). RRO is a disturbance where frequency is synchronized with the spindle rotation frequency, or one of its multiples. The repeatable nature of an imperfect track producing the runout motion that is locked to the spindle rotation in both frequency and phase, is the major source of RROs stemming from the eccentricity of the track. Other sources include bearing geometry and motor geometry. The major source of NRRO is external shock. Other sources include electrical noise and wind-induced vibration. Usually the RRO magnitude is higher than that of NRRO.

In existing literature, hard disk drive's track following control technique uses either adaptive or robust control algorithms or both to handle external disturbance and model uncertainties.

DSA's increase system bandwidth and error/disturbance response, thus improving following performance. Kemao Peng, Ben M. Chen , Tong H. Lee and V. Venkataramanan (2004)[4] proposed a dual stage actuator that was able to improve the performance of response and track following more than a single stage actuator based on composite nonlinear control approach. Hidehiko and Masayoshi (2003) [3] presented a settling control of a dual-actuator system for hard disk drives. The decoupling filter, which is placed between the voice-coil motor (VCM) controller input and the PZT controller output, is a PZT output estimator so that the PZT actuator output is canceled at the VCM controller input. Taghirad and Jamei (2008) [15] applied an adaptive robust control, originated by Yao (1997), to a hard disk drive. Zheng and Tomizuka (2007) [18] proposed an adaptive compensation scheme to estimate and compensate the dominant frequency component in the NRRO. Most of the adaptive algorithms are computationally intensive and have yet to prove their practicality on experiments.

Du et al. (2008)[9] devised a linear controller based on solving linear matrix inequalities, a method proposed by Boyd et al. (1994), for actuator positioning. The disturbance is rejected using an adaptive nonlinear compensation. You and Hong (2007) [17] proposed a robust sliding mode control with a new switching surface for track following. Low and Wong (2007)[12] used multi-objective genetic algorithm in a controller-tuning scheme for a hard disk drive servo system by placing constraint objectives at high priority than the

optimization objectives. Park et al. (2005)[14] presented a hard disk drive servo control based on repetitive control algorithm, proposed in Hara et al. (1988.)

In this paper, we propose a control system for hard disk drive track following given in the benchmark problem by Chen et al. (2006.)[2] The method is based on quantitative feedback theory, devised by Horowitz (1959.)[10]. Model uncertainties are considered explicitly during the control design process. Other specifications such as disturbance rejection, tracking, and stability can be specified to ensure that the resulting control system meets or exceeds these requirements.

II. DUAL STAGE ACTUATOR MODEL

This paper studies a dual-stage HDD with a push–pull PZT micro-actuator as shown in Fig. 1.

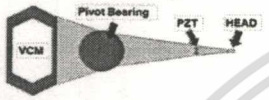

Fig 1. Drawing of a VCM with amounted PZT

Dual stage actuators consist of two actuators. The first actuator is the VCM and the second actuator is PZT, which is mounted on active suspension. The frequency responses of VCM and PZT were measured from displacement of head when injected the sweep sine source at frequency range of drive operation.

The model of VCM and PZT can be present in equation by

$$G_{rigid} \approx \frac{\omega_p^2}{S^2+2\zeta\omega_p S+\omega_p^2}$$

$$\mathrm{Re}\, s \approx \prod_{i=1}^{n} \frac{S^2+2\zeta_{zi}\omega_{zi}S+\omega_{zi}^2}{S^2+2\zeta_{pi}\omega_{pi}S+\omega_{pi}^2} \quad (1)$$

The model of VCM and PZT have been attenuate resonance frequency by notch filler for stabilize of system. The notch have represented the equation by

$$N(s) \approx \prod_{i=1}^{n} \left(\frac{\omega_{pi}^2}{\omega_{zi}^2}\right)\left(\frac{S^2+2\zeta_{zi}\omega_{zi}S+\omega_{zi}^2}{S^2+2\zeta_{pi}\omega_{pi}S+\omega_{pi}^2}\right) \quad (2)$$

Fig. 2 has showed the comparison between plant VCM and PZT with and without notch.

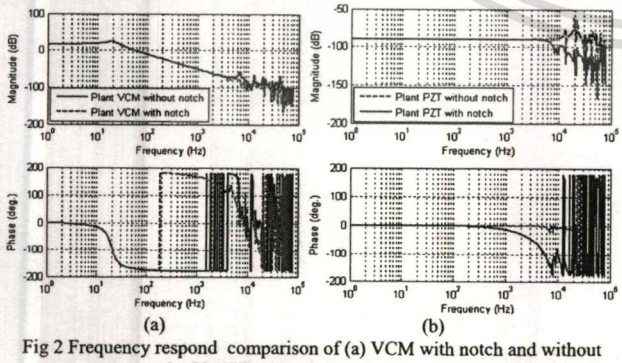

Fig 2 Frequency respond comparison of (a) VCM with notch and without notch. (b) PZT with notch and without notch.

The objective is to design a control system such that the actual displacement of the head tracks a reference when the following specifications are met:

1. The overshoot of the actual displacement is less than 5%;
2. The mean of the steady-state error is zero;
3. The gain and phase margins are greater than 6dB and 30°;
4. The maximum peaks of the sensitivity are less than 10dB;
5. The 50% settling time of the step response is as short as possible.

III. CONTROLLER DESIGN

The controller system prefers block diagram in Fig. 3. The G_v is VCM plant and series with N_v, which is notch filler for system stabilize and C_v is controller for compensate of VCM plant. The PZT loop, there is G_p is plant of PZT and N_p is notch filler for stability of plant PZT and C_p is compensator of PZT plant, final blocks is $\hat{G}_p$ decoupling filter, which is placed between the VCM controller input and the PZT controller output, is a PZT output estimator so that the PZT actuator output is canceled at the VCM controller input. The P_{ref} is input command for DSA actuator move the head go to the target, which track following approach assume is zero, that mean head stay on the center track. The TMR is disturbance source consist of NRRO and RRO. PES (Position Error Signal), which is input to the controller.

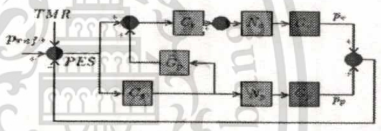

Fig 3 Block diagram of DSA with decoupling

From block diagram, the open loop gain is showed in by

$$Go(s) = CvNvGv + CpNpGp + Cp\hat{G}pCvNvGv \quad (3)$$

Assume $\hat{G}_p = N_p G_p$ then rewrite by

$$Go(s) = CvNvGv(1 + CpNpGp) + CpNpGp \quad (4)$$

In term of sensitivity, that able be write by

$$S(s) = \frac{1}{1+Go} = \frac{1}{(1+CvNvGv)(1+GpNpGp)} \quad (5)$$

Or

$$S(s) = \frac{1}{(1+Gvo)(1+Gpo)} \quad (6)$$

So from equation (6), the sensitivity function can be compute by individual loop between VCM and PZT, then combine both by add $\hat{G}_p$ compensator. The VCM loop shaping is use quantitative feedback theory firstly, compute the uncertainty plant and plot thought plant temple, which is show in Fig. 4.

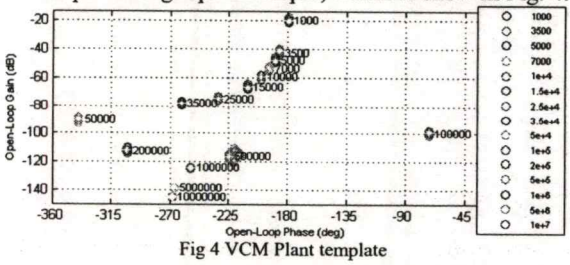

Fig 4 VCM Plant template

Secondly, Compute open loop transfer function and sensitivity function from uncertainty plant and plot thought Nichol chart, the intersection of plot, which will be used for compensator loop shaping. Fig. 5 is showed (a) is before loop shaping, that found nominal plant pass in thought unstable region than tuning the compensator. The result is showed on Fig. 5(b)

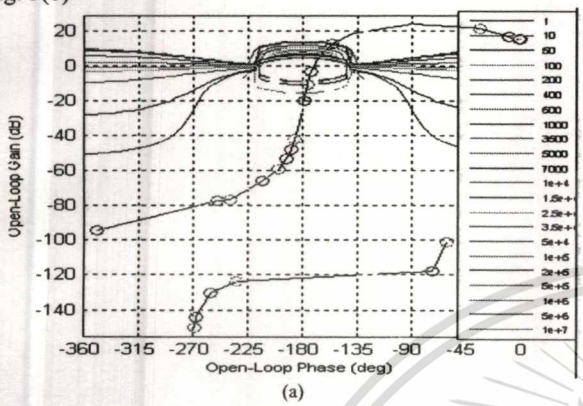

(a)

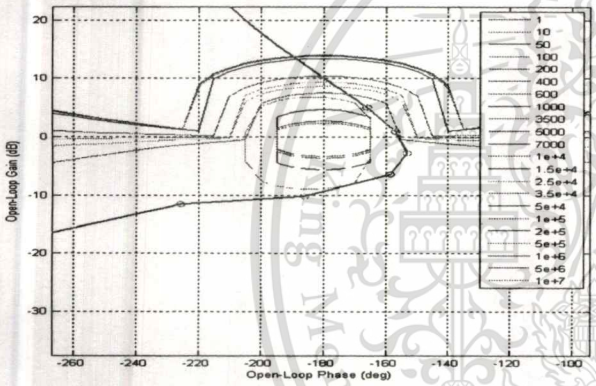

(b)

Figs 5 VCM loop shaping. (a) Before loop shaping. (b)After loop shaping.

The compensator after loop shaping, which is show by

$$Cv(s)=\frac{2138S^5+4.149x10^8S^4+6.882x10^{13}S^3+3.084x10^{18}S^2+1.688x10^{22}S+2.354x10^{25}}{S^5+1.983x10^5S^4+3.563x10^{10}S^3+1.701x10^{15}S^2+4.215x10^{19}S} \quad (7)$$

The PZT compensator is use lead-lag technique for handle system stability the PZT compensator is showed by

$$Cp(s)=\frac{2.046x10^4S^4+8.635x10^9S^3+1.413x10^{15}S^2+1.619x10^{22}S+3.857x10^{24}}{S^4+4.021x10^5S^3+6.247x10^{10}S^2+6.916x10^{15}S+1.993x10^{19}} \quad (8)$$

Two specifications are tracking and plant-output disturbance rejection. For tracking, we use

$$\alpha \le \left|\frac{P_oC_oF}{1+P_oC_o}\right| \le \beta \quad (9)$$

Where P_o represents the product of the nominal plant, the resonant modes with the notch filters, Co is the controller, F is the prefilter. α and β are two transfer functions in the form $\omega_n^2/\left(s^2+2\zeta\omega_n s+\omega_n^2\right)$ with $\{\omega_n,\zeta\}=\{1x10^4,1\}$ and $\{\omega_n,\zeta\}=\{1x10^4,0.7\}$ respectively. For plant-output disturbance rejection, use

$$\left|\frac{1}{1+P_oC_o}\right| < \delta_{dO} \quad (10)$$

Where δdo is set to 10dB. It can be shown that the plant-output disturbance rejection is indeed a stability margin specification.

Thirty, estimation $\hat{G}_p$ from $\hat{G}_p = N_pG_p$ for decoupling loop

Finally used closed-loop shaping to find a prefilter F The controller just makes the variation in the closed-loop shape to be within specified upper and lower tracking bounds. The prefilter F is then designed to adjust the gains to be within the tracking bounds. The lower and upper tracking bounds is α and β respectively, the prefilter is

$$F(s)=\frac{0.4577S^3+4755S^2+3.38x10^7S+1.493x10^{11}}{S^3+10047S^2+7.033x10^7S+1.493x10^{11}} \quad (11)$$

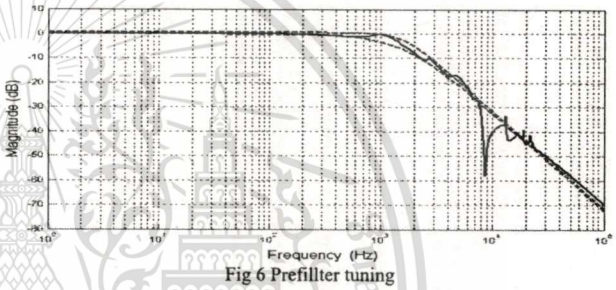

Fig 6 Prefillter tuning

IV. Simulation Results

In summary result, the QFT control system has meeting most of the specifications required by the specification. The PID gain value is come from normalize value and comparison disturbance rejection between measurement and simulation.

First, the overshoot of the actual displacement head is less than 5% as shown in Fig. 9. Second, the steady-state error is zero as shown in Fig. 9. Third, the gain margin and phase margin is 8.7 dB and 57° respectively, that show in Fig. 7.Fourth, the maximum peaks of the sensitivity function is less than 10 dB in most frequencies, that present is Fig.8 Fifth, the QFT control system achieves faster 50% settling time of the step response the PID controllers, which is show in Fig. 9.Final, Finally, the RRO disturbance rejection of the QFT is about thirty times better than the PID technique, that is showed in Fig.10.

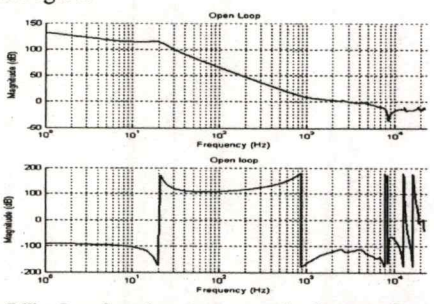

Fig 7 The Open loop frequency responds of system after tuning

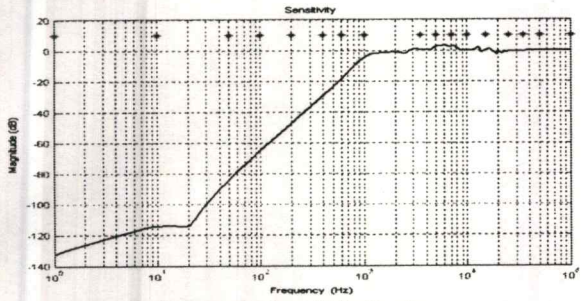

Fig 8 The result of sensitivity function

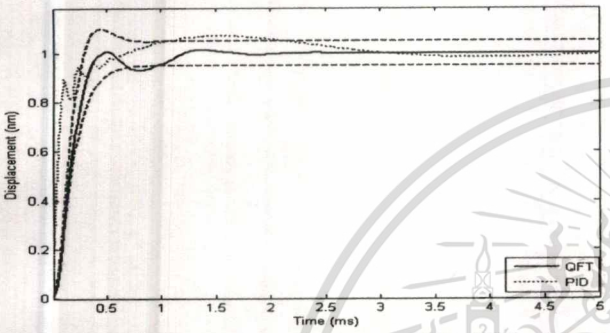

Fig 9 The head displacement comparison between QFT and PID technique.

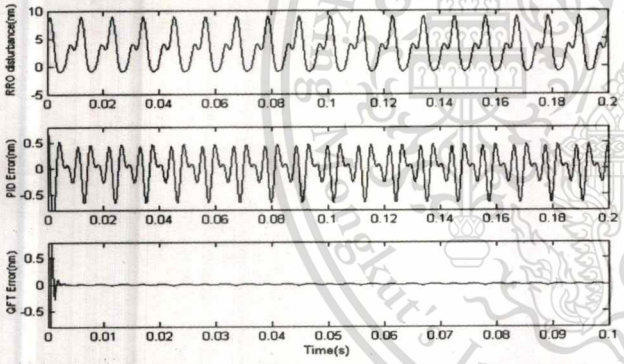

Fig 10 The RRO disturbance rejection comparison between PID and QFT technique.

V. Conclusion

The simulation result of quantitative feedback system can be covered in boundary of Nichols charts and the loop shaping can be shaped to ensure that the resulting control system meets all essential specifications. The method presented in this paper can also be applied to improve the performance of the dual-stage actuator even further.

Acknowledgment

The authors would like to thank Western Digital (Thailand) Co., Ltd. for providing some technical assistance and financial support. We would also like to thank Craig Borghesani and Terasoft, Inc for their evaluation copy of the QFT Matlab toolbox.

References

[1] A. Al Mamun, T. H. Lee, and T. S. Low, "Frequency domain identification of transfer function model of a disk drive actuator," *Mechatronics,* vol. 12, pp. 563-574, May 2002.

[2] G. Y. Cheng, K. M. Peng, B. M. Chen, and T. H. Lee, "A microdrive track following controller design using robust and perfect tracking control with nonlinear compensation," *Mechatronics,* vol. 15, pp. 933-948, Oct 2005.

[3] H. Numasato and M. Tomizuka, "Settling control and performance of a dual-actuator system for hard disk drives," *Ieee-Asme Transactions on Mechatronics,* vol. 8, pp. 431-438, Dec 2003.

[4] K. Peng, B. M. Chen, T. H. Lee, and V. Venkataramanan, "Design and implementation of a dual-stage actuated HDD servo system via composite nonlinear control approach," *Mechatronics,* vol. 14, pp. 965-988, Nov 2004.

[5] K. C. Tan, R. Sathikannan, W. W. Tan, and A. P. Loh, "Evolutionary design and implementation of a hard disk drive servo control system," *Soft Computing,* vol. 11, pp. 131-139, Jan 2007.

[6] M. Vagia, G. Nikolakopoulos, and A. Tzes, "Design of a robust PID-control switching scheme for an electrostatic micro-actuator," *Control Engineering Practice,* vol. 16, pp. 1321-1328, Nov 2008.

[7] Yamaguchi, T.; "HDD servo control development - Present and future" SICE-ICASE, 2006. International Joint Conference Publication Year: 2006 , Page(s): 2756 - 2759 [1-6]

[8] Shangying Zhang; Xuedong Chen; Haihua Mu; Hui Zhao; "Quantitative feedback control of a linear positioning stage with cogging force compensation" Nano/Micro Engineered and Molecular Systems, 2008. NEMS 2008. 3rd IEEE International Conference on Publication Year: 2008 , Page(s): 660 – 663

[9] Du, C., L. Xie, J. Zhang, and G. Guo. 2008. Disturbance Rejection for a Data Storage System via Sensitivity Loop Shaping and Adaptive Nonlinear Compensation. IEEE/ASME Transactions on Mechatronics. Vol. 13. No. 5. pp. 493-501.

[10] Horowitz, I. 1959. Fundamental Theory of Linear Feedback Control Systems. Trans IRE on Auto Control. AC-4.

[11] Levin, J. and P. Ioannou. 2009. Adaptive Mode-Suppression and Disturbance-Rejection Scheme with Application to Disk Drives. IEEE Transactions on Control Systems Technology. Vol. 17. No. 3. pp. 620-632.

[12] Low, K.S. and T.S. Wong. 2007. A Multiobjective Genetic Algorithm for Optimizing the Performance of Hard Disk Drive Motion Control System. IEEE Transactions on Industrial Electronics. Vol. 54. No. 3. pp. 1716-1725.

[13] Ohno, K. and T. Hara. 2006. Adaptive Resonant Mode Compensation for Hard Disk Drives. IEEE Transactions on Industrial Electronics. Vol. 53. No. 2. pp. 624-630.

[14] Park, S.W., J. Jeong, H.S. Yang, Y.P. Park, and N.C. Park. 2005. Repetitive Controller Design for Minimum Track Misregistration in Hard Disk Drives. IEEE Transactions on Magnetics. Vol. 41. No. 9. pp. 2522-2528.

[15] Taghirad, H.D. and E. Jamei. 2008. Robust Performance Verification of Adaptive Robust Controller for Hard Disk Drives. IEEE Transactions on Industrial Electronics. Vol. 55. No. 1. pp. 448-456.

[16] Yao, B. 1997. High Performance Adaptive Robust Control of Nonlinear Systems: A General Framework and New Schemes. Proc IEEE Conf Decision Control. San Diego. CA. pp. 2489-2494.

[17] You, K.H. and M. Hong. 2007. Robust Linear Quadratic Sliding-Mode Control for Hard Disk Drives. IEEE Transactions on Instrumentation and Measurement. Vol. 56. No. 3. pp. 1087-1093.

[18] Zheng, Q. and M. Tomizuka. 2007. Compensation of Dominant Frequency Components of Nonrepeatable Disturbance in Hard Disk Drives. IEEE Transactions on Magnetics. Vol. 43. No. 9. pp. 3756-3762.

BIOGRAPHY

Name: Mr. Taweesak Aryurawattana

Date of Birth: 23 February 1980

Place of Birth: Samutpharkan, Thailand

Address: 53/97 Krungmeang Village, Srinakarin Road, Bangkeaw, Bangpee, Samutpharkan, 10540

Education:

1999-2003 Bachelor degree, Faculty of Engineering King Mongkut's Institute of Technology North Bangkok , Majoring in Electrical Engineering.

Work Experience:

2003-2007 R&D Engineering at Thai Samsung Electronics (Thailand) Co., Ltd.

2007-Now Servo Engineering at Western Digital (Thailand) Co., Ltd.

Scholarships:

2009-2013 Scholarship for study in the Master degree from Data Storage Technology and Innovations, King Mongkut's Institute of Technology Ladkrabang.

Publications:

T. Aryurawattana, W. Chatlatanagulchai, and U. Pinsopon "Track Following Control of HDD Dual Stage Actuator UsingQuantitative Feedback Theory," The 5th International Data Storage Technology Conference. Thailand – Conference, February14-15, 2013.